© 2020. Published by The Company of Biologists Ltd | Journal of Cell Science (2020) 133, jcs227355. doi:10.1242/jcs.227355

RESEARCH ARTICLE

Disc-associated proteins mediate the unusual hyperstability of the ventral disc in *Giardia lamblia*

Christopher Nosala*, Kari D. Hagen*, Nicholas Hilton*, Tiffany M. Chase, Kelci Jones, Rita Loudermilk, Kristofer Nguyen and Scott C. Dawson‡

ABSTRACT

Giardia lamblia, a widespread parasitic protozoan, attaches to the host gastrointestinal epithelium by using the ventral disc, a complex microtubule (MT) organelle. The 'cup-like' disc is formed by a spiral MT array that scaffolds numerous disc-associated proteins (DAPs) and higher-order protein complexes. In interphase, the disc is hyperstable and has limited MT dynamics; however, it remains unclear how DAPs confer these properties. To investigate mechanisms of hyperstability, we confirmed the disc-specific localization of over 50 new DAPs identified by using both a disc proteome and an ongoing GFP localization screen. DAPs localize to specific disc regions and many lack similarity to known proteins. By screening 14 CRISPRi-mediated DAP knockdown (KD) strains for defects in hyperstability and MT dynamics, we identified two strains – DAP5188KD and DAP6751KD – with discs that dissociate following high-salt fractionation. Discs in the DAP5188KD strain were also sensitive to treatment with the MT-polymerization inhibitor nocodazole. Thus, we confirm here that at least two of the 87 known DAPs confer hyperstable properties to the disc MTs, and we anticipate that other DAPs contribute to disc MT stability, nucleation and assembly.

KEY WORDS: Giardia, Microtubule-associated protein, MAP, Microtubule inner protein, MIP, Microtubule, Organelle

INTRODUCTION

Many microbial eukaryotes possess complex interphase microtubule (MT) organelles that offer a unique perspective into the abilities of MT polymers to generate diverse forms and functions in cells. Such MT organelles are often defined by intricate higher order MT assemblies and contain proteins that lack similarity to well-studied MT-binding proteins in other eukaryotes (Hagen et al., 2011; Hu et al., 2006; Preisner et al., 2016). Novel MT-associated proteins may provide structural stability, facilitate organelle motility or have unknown functions required for organelle synthesis or maintenance.

The widespread protistan intestinal parasite *Giardia lamblia* is defined by one such elaborate MT organelle, the cup-shaped ventral disc (Crossley and Holberton, 1983a, 1985; Feely et al., 1982; Friend, 1966; Holberton, 1973, 1981). Infectious *G. lamblia* cysts are commonly ingested from contaminated water (Einarsson et al., 2016) and excyst into flagellated trophozoites. Using the ventral disc, trophozoites attach to the intestinal microvilli to resist being dislodged by peristalsis (Elmendorf et al., 2003; Nosala and Dawson, 2015). Colonization leads to acute or chronic diarrheal disease in humans and other animals (Nosala and Dawson, 2015). Although the molecular mechanisms of attachment are not well understood, *G. lamblia* trophozoites are thought to attach through hydrodynamic suction-based forces that result in a pressure differential underneath the disc relative to the outside medium (Hansen et al., 2006; Holberton, 1974). Conformational changes of regions of the disc may also create or modulate attachment forces (Dawson et al., 2007; Woessner and Dawson, 2012).

The parallel MTs of the ventral disc scaffold an intricate architecture of associated structural elements (Fig. 1) first described over 50 years ago (Cheissin, 1964; Friend, 1966). Approximately 100 uniformly spaced, singlet disc MTs spiral one-and-a-quarter turns to form a domed organelle 8 µm in diameter (Brown et al., 2016). An overlap zone occurs between the upper and lower parts of the spiral, and a raised ventral groove region lies adjacent to the ventral flagella (Fig. 1A,B,E). An associated structure at the disc periphery, the lateral crest (Fig. 1C), forms a seal with surfaces in early attachment (Feely et al., 1990, 1982; House et al., 2011). Overall, the disc MTs comprise >1.2 mm of polymerized tubulin (Brown et al., 2016), yet the disc MT array is unaffected by treatment with the MT-polymerization inhibitor nocodazole or the MT stabilizer Taxol (Dawson et al., 2007), implying that it is a stable structure with limited interphase MT dynamics.

The first 3D high-resolution structure was obtained using cryo-electron tomography (cryo-ET) of whole isolated ventral discs with sub-tomogram averaging (Schwartz et al., 2012). The work by Schwartz and colleagues further articulated the elaborate cytoskeletal architecture, which is highlighted by repetitive complexes comprising microribbons (MRs) and crossbridges (CBs) that coat almost every protofilament of the MT spiral array (Fig. 1). Unusual, yet regularly-spaced, microtubule-associated protein (MAP) complexes (e.g. sidearms and paddles) (Fig. 1A) and three protein densities associated with the MT lumen – i.e. the MT inner proteins (MIPs) *g*MIP5, *g*MIP7 and *g*MIP8 – were also defined (Schwartz et al., 2012).

Interphase MT organelles in protists represent an untapped reservoir of non-canonical MT-binding proteins that may govern MT assembly, nucleation or dynamics (Dawson and Paredez, 2013). Although a handful of disc-associated proteins (DAPs) termed 'giardins' were isolated from the disc two decades after the initial disc structures had been described (Crossley and Holberton, 1983a), the identities of many of the proteins composing the unique MT-associated disc structure remained elusive. In a comprehensive proteomic analysis of detergent-extracted, isolated ventral discs, we have previously identified nearly twenty new DAPs that localize to regions of the ventral disc or lateral crest (Hagen et al., 2011).

Department of Microbiology and Molecular Genetics, University of California, Davis, One Shields Avenue, Davis, CA 95616, USA.
*These authors contributed equally to this work

‡Author for correspondence (scdawson@ucdavis.edu)

C.N., 0000-0002-0179-8101; K.D.H., 0000-0001-9673-2481; T.M.C., 0000-0001-9931-7697; R.L., 0000-0001-9970-5112; K.N., 0000-0001-8520-4835; S.C.D., 0000-0002-0843-1759

Handling Editor: David Stephens
Received 31 October 2018; Accepted 29 June 2020

Journal of Cell Science (2020) 133, jcs227355. doi:10.1242/jcs.227355

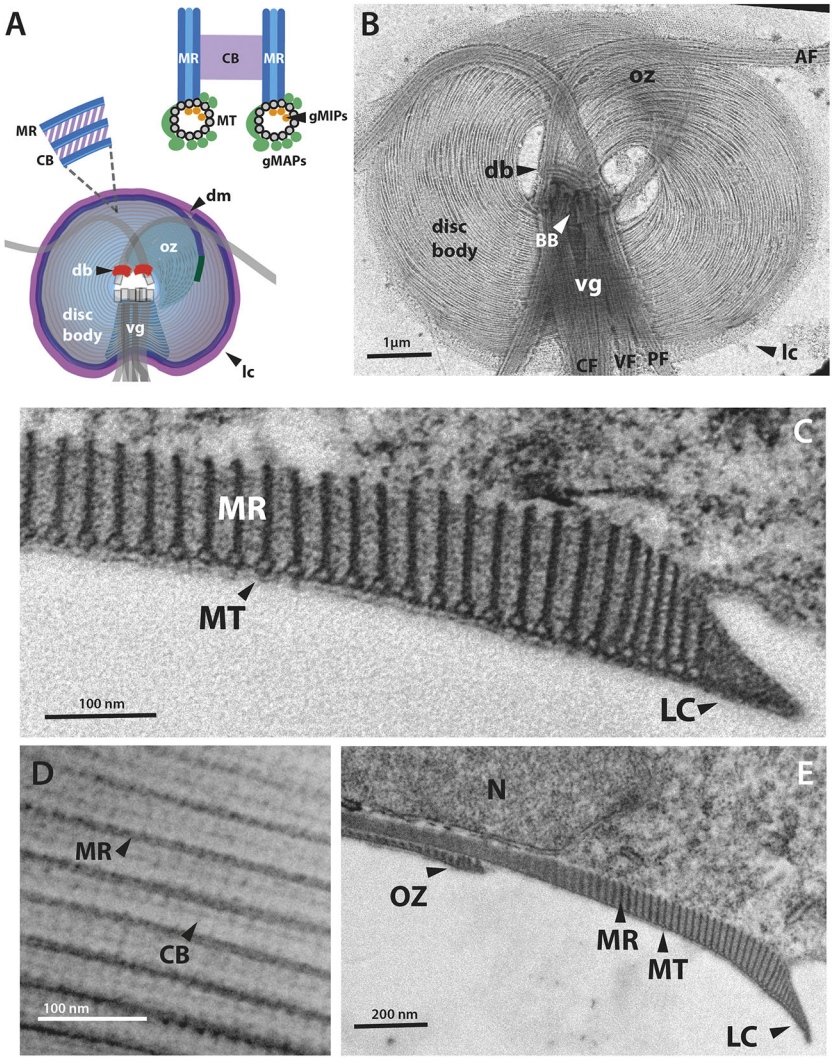

Fig. 1. Elaborate and unique protein complexes associated with the disc microtubule array. (A) Schematic of the ventral disc indicating the primary structural elements, including the disc MT array (disc body), disc margin (dm), dense bands (db), overlap zone (oz), ventral groove (vg), and lateral crest (lc). The inset shows a cross section of the MR–CB complex (MT, microtubules; MR, microribbons; CB, crossbridges) and the *G. lamblia* MAPs (*g*MAPs, green) or MIPs (gMIPs, orange). (B) Negative-stained cytoskeletal preparation of the ventral disc, highlighting the primary structural elements, basal bodies (BB), and regions of the eight cytoplasmic axonemes (AF, anterior flagella; CF, caudal flagella; PF, posteriolateral flagella; VF, ventral flagella). (C) Transmission electron microscopy of thin sections of whole embedded trophozoites showing the lateral crest (LC) and microribbons (MRs) associated with each MT of the spiral array. (D) Negative-stained preparation of the disc highlighting MRs linked to regularly spaced crossbridges (CBs). (E) The overlap zone (OZ) of the MT spiral array, together with the MR–CB complexes, are shown in cross section (N, nucleus).

Despite our emerging view of the complexity of ventral disc architecture and composition (Brown et al., 2016), we still know little about the functional basis of the unusual stability and limited MT dynamics of the disc. Thirty-four DAPs have been identified previously by using proteomic or protein-tagging approaches (Davids et al., 2008; Ebneter and Hehl, 2014; Ellis et al., 2003; Hagen et al., 2011; Lauwaet et al., 2007, 2011; Lourenço et al., 2012; Palm et al., 2005; Weiland et al., 2005). Combining a new disc proteome with a high-throughput GFP-tagging approach, we now identify an additional 53 DAPs, bringing the total number of confirmed DAPs to 87. Approximately two-thirds of all DAPs localize exclusively to the disc; the remainder also localize to other MT organelles, such as the flagella or median body. Some DAPs are conserved homologs of MAPs and MIPs (Nosala et al., 2018) known to stabilize ciliary doublet and triplet MTs (Ichikawa and Bui, 2018; Stoddard et al., 2018). Most DAPs, however, lack identifiable MT-binding domains; thus, the disc is primarily composed of proteins with ankyrin-repeat domains or proteins that lack similarity to other proteins in diverse eukaryotes.

Molecular genetics and functional analyses of the newly identified DAPs are central to understand the overall disc architecture, assembly and dynamics. Many of these DAPs are likely to stabilize singlet MTs in the spiral array or limit interphase disc MT dynamics. Here, we confirm that specific DAPs are required to confer the unusual hyperstable properties of the disc that limit MT dynamics during interphase. Although we have previously reported that the disc is insensitive to MT drugs (Dawson et al., 2007), we show here that CRISPRi-mediated knockdown (KD) of the ankyrin-repeat-containing DAP5188 causes the disc to become sensitive to the MT-polymerization inhibitor nocodazole. Moreover, KD of either DAP5188 or the novel protein DAP6571 causes ventral discs to lose some of their hyperstable properties and to dissociate during high-salt extraction. We anticipate that other recently identified DAPs – together with conserved MAPs and MIPs that are known to stabilize MTs – also confer hyperstable properties to the disc, which are required for its function of attachment to the host.

RESULTS

Biochemical fractionation and shotgun proteomic analysis of the *G. lamblia* cytoskeleton enabled the identification of over 50 new DAPs

Detergent extraction of trophozoites removes the membrane and cytosol, resulting in isolation of the entire MT cytoskeleton, including intact ventral discs and axonemes (Fig. 1B). This cytoskeletal preparation is stable in PHEM buffer for weeks (Crossley and Holberton, 1983a,b, 1985; Holberton and Ward, 1981). By using cryo-ET of such detergent-extracted cytoskeletons,

Journal of Cell Science (2020) 133, jcs227355. doi:10.1242/jcs.227355

Brown et al. have recently defined specific variations of the ventral disc architecture in the ventral groove, disc margin and overlap zone regions (Fig. 1) (Brown et al., 2016). We hypothesized that the protein density disparities observed in these distinct disc regions represent the targeting of specific DAPs to these regions.

To attempt to dissociate DAPs that confer disc structural stability or integrity, we modified a prior biochemical fractionation protocol and disrupted the cytoskeleton to obtain a disc-enriched fraction (Crossley and Holberton, 1983b; Holberton and Ward, 1981). Ventral discs were extracted with 1% Triton X-100 and 1 M KCl (Fig. S1), which facilitated the removal of contaminating proteins associated with the nuclei and cytosol, as observed by negative-staining EM. The disc and flagellar cytoskeletons (and occasionally median bodies) were retained following this high-salt extraction (Fig. S1B). Negative staining of the P1 fraction (Fig. S1D) showed loss of the majority of nuclei and retention of the disc, flagella and funis. Subsequent extractions alternating Tris-EDTA and HEPES buffers destabilized and released the disc from the axonemes and basal bodies, resulting in supernatant or pellet fractions (S2, P2, S3 and P3). These additional treatments produced a fraction enriched for ventral discs (fraction S3, Fig. S1E,F) and resulted in relaxation of the normally domed, closed ventral disc spiral (Fig. S1E,F). Many structural components of flagella were also removed in fraction S3 (Fig. S1E,F and Table S1). SDS-PAGE resolved proteins enriched in each pellet (P1, P2, P3) and supernatant (S2, S3) fraction (Fig. S1G).

Proteomic analysis of fractions enriched in ventral disc or flagellar proteins

The compositions of the initial cytoskeletal preparation (P1), two supernatant fractions (S2, S3) and the final pellet remaining after extraction (P3) were determined by mass spectrometry. Proteins with fewer than five peptides were excluded and the four fractions were compared (Fig. S1H and Table S1). One hundred and fifty-seven proteins were identified with at least five peptides in any fraction (Table S1). Tubulins, giardins, median body protein and GASP-180 family proteins were among the most commonly identified proteins. Thirty-five proteins (33 DAPs, one α- and one β-tubulin isoform) occurred in every fraction examined. The 33 DAPs included three striated fiber (SF)–assemblins (β-giardin, δ-giardin and SALP-1) (Baker et al., 1988; Jenkins et al., 2009; Palm et al., 2005), the MR protein γ-giardin (Kim and Park, 2019; Nohria et al., 1992), 11 ankyrin-repeat proteins and 14 DAPs without any known motifs (Table S1). Ten DAPs were unique to the P1 fraction; 24 proteins were enriched in the S2 fraction and nine were enriched in the P3 fraction as compared to other fractions.

Tagging of selected proteins allowed us to identify new DAPs. Forty-nine DAPs were present in the P1, S2 or S3 fractions. Although no DAPs were exclusive to the S3 fraction (Fig. S1H and Table S1), 25 proteins in the S3 fraction had disc localization and only four localized to the flagella. Approximately three quarters of the 22 confirmed flagellum-localizing proteins (basal bodies or axonemes) were present in the P1 or S2 fractions only. Lateral crest DAPs were primarily in the P1 fraction. Twenty-three DAPs identified and confirmed in this proteome had also been identified in prior disc-enriched proteome studies (Hagen et al., 2011; Lourenço et al., 2012) (Table S2). Three DAPs had been identified in other cytoskeletal proteomes (Lauwaet et al., 2011). Thirty-five DAPs had been previously identified solely by localization-based tagging methods (Davids et al., 2008; Ebneter and Hehl, 2014; Ellis et al., 2003; Hagen et al., 2011; Lauwaet et al., 2007, 2011; Palm et al., 2005; Weiland et al., 2005). Twenty-six DAPs had been identified exclusively in the ongoing GFP-tagging project of our laboratory (Nosala et al., 2018), yet were below a threshold abundance in the disc-enriched proteome (Tables S1 and S2). The 35 DAPs that lack current proteomic support were, nonetheless, included in subsequent analyses of ventral disc composition (Figs 2 and 3; Table S2).

A revised inventory of disc-associated proteins that lack known MT-binding motifs

To determine the subcellular localization of new candidate DAPs, we fused GFP to the C-terminal end of each protein and expressed the candidate DAP-GFP fusions using their native promoters (Figs 2, 3 and Figs S2–5). The disc-specific localization of 53 new DAPs was confirmed, bringing the total number of verified DAPs to 87 (Fig. 2A and Table S2). Only two of these 87 DAPs possess known outer MT-binding motifs (Fig. 2B and Table S2). One is kinesin-6a (DAP102455), which localized to the disc margin region and is the only kinesin associated with the disc. The other, DAP5374, has a CAP-GLY domain (Weisbrich et al., 2007) and localized to four disc regions (Fig. 2B and Table S2). Of the remaining confirmed DAPs, 25 lack similarity to any known protein in other eukaryotes (Fig. 2B). Each novel protein has a distinct localization pattern; not all localize to the same disc or lateral crest region. An additional 27 DAPs contain only predicted ankyrin-repeat domains (Fig. 2B and Table S2) and, like the novel proteins, were found in various regions of the disc. Several DAPs are members of conserved protein families, including: three SF-assemblins (Palm et al., 2003); four annexins, e.g. α-giardins (Bauer et al., 1999; Peattie, 1990; Weiland et al., 2005, 2003) and 13 NEK kinases (Fig. 2 and Table S2). Nine of the 13 NEKs lack conserved catalytic residues (Nosala et al., 2018). Other DAPs include those possessing a WD40-repeat domain (DAP15218), a DUF1126 domain (DAP41512), an Mlf1IP domain (DAP16424), an ENTH domain (DAP3256) (Ebneter and Hehl, 2014) or SHIPPO-repeat domains (DAP103164 and DAP9148).

DAP localization to other MT organelles and to distinct ventral disc regions

Forty-two of the 87 known DAPs localized only to specific regions of the ventral disc and not to other cytoskeletal structures (Fig. 2C). However, many of the newly identified DAPs localized to the disc and to at least one other MT structure, including the median body (Fig. 2D,F; 23 DAPs in total), the eight axonemes and basal bodies (Fig. 2E,F,H; 31 DAPs in total), or the lateral crest, a repetitive structure separate from the disc that surrounds the disc MT array (Fig. 2G,H; four DAPs in total). Eleven DAPs localized to all of the primary MT-based structures including the disc, flagella and median body (Fig. 2F).

Because ventral disc-specific GFP localization patterns varied, we further categorized the localizations of all 87 DAP-GFP strains, defining five distinct regions within the disc itself: the disc body, the disc margin, the overlap zone, the ventral groove and the dense bands (Fig. 3 and Table S2). The majority of the 87 DAPs localized to more than one disc region: 44 DAPs localized to the disc body, 37 DAPs to the disc margin, 34 DAPs to the overlap zone, 33 DAPs to the ventral groove and seven DAPs to the dense bands (Fig. 3 and Table S2). Thirty-six of the 87 DAPs localized to only one of the disc regions: six DAPs localized to the disc body only, three localized to the overlap zone only, 21 to the disc margin, four to the dense bands and two localized only to the ventral groove. Although six DAPs in total localized to the lateral crest, only two localized solely to the lateral crest and not to other disc or cytoskeletal elements (Fig. 2 and Table S2). There are also subtle, yet noticeable,

Journal of Cell Science (2020) 133, jcs227355. doi:10.1242/jcs.227355

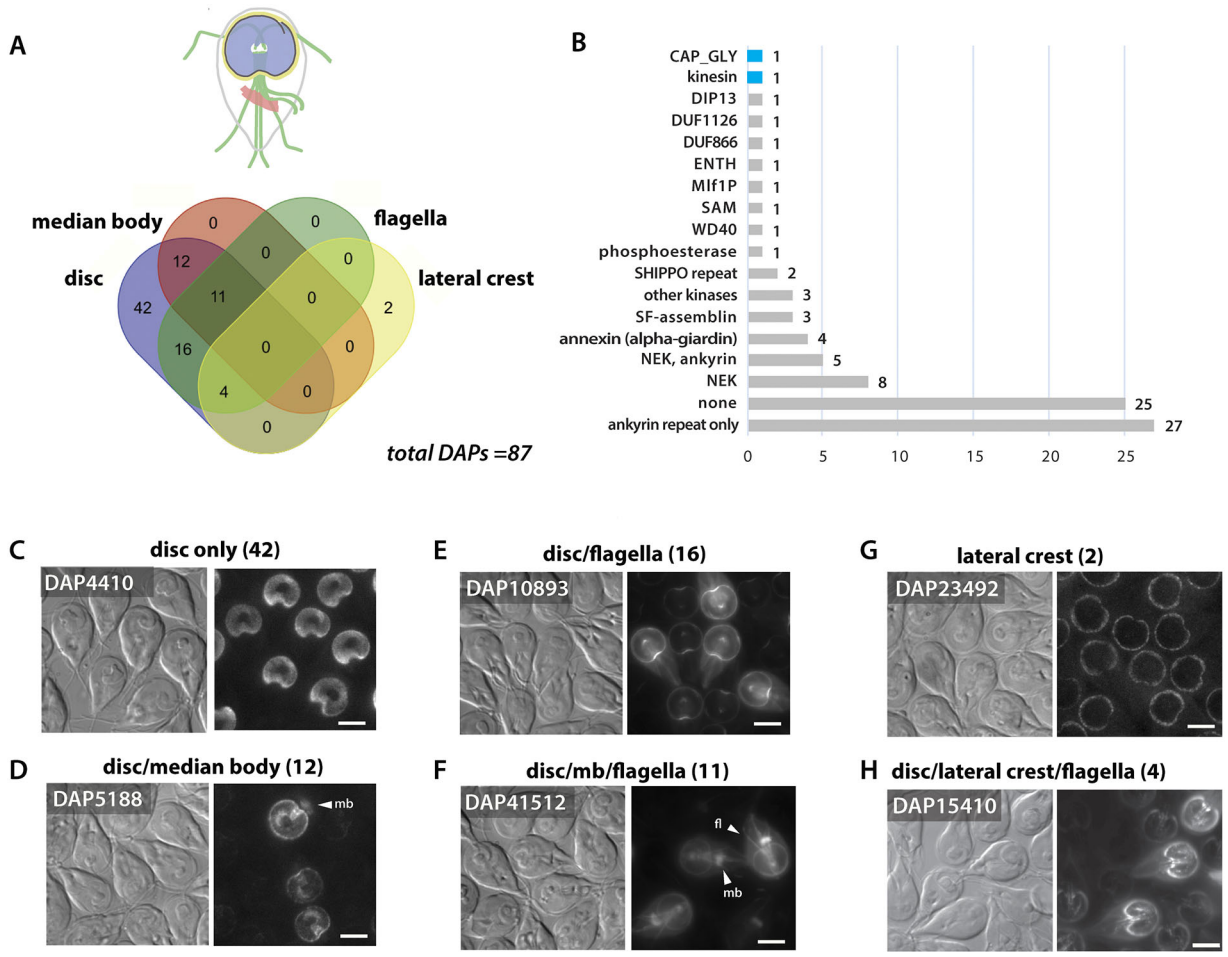

Fig. 2. Disc-associated proteins localize to dynamic and to stable MT organelles. The subcellular localizations of 87 DAP C-terminal GFP fusion proteins identified by fractionation and mass spectrometry (Fig. S1) were categorized. (A) Venn diagram indicating DAPs with overlapping localizations to the disc, flagella, median body and lateral crest. Some DAPs localized exclusively to the disc (*n*=42), whereas others localized to both the disc and other cytoskeletal structures, including the flagella (*n*=31), median body (*n*=12) and lateral crest (*n*=4). (B) PFAM domains of the 87 confirmed *G. lamblia* DAPs were summarized and ranked by abundance. A CAP_GLY domain (blue) and a kinesin motor domain (blue) are the only known MT-binding motifs that were identified in the 87 DAPs. (C–F) Representative localizations are shown for 42 DAPs localizing solely to the disc (C), for the 12 DAPs localizing to both the disc and median body (mb) (D), the 16 DAPs localizing to both the disc and flagella (fl) (E), and the 11 DAPs localizing to the disc, median body and flagella (F). (G) Two DAPs localized only to the lateral crest. (H) Four DAPs localized to the lateral crest, disc, and flagella. The flagella category includes localizations to the basal bodies and/or the cytoplasmic or membrane-bound regions of the flagella. Scale bars: 5 µm.

variations in localizations within any particular disc region in the DAP-GFP strains; for example, some strains with disc body or disc margin localizations lacked localization at the ventral groove region (Figs S2–S5).

Using CRISPRi-mediated KD to identify new DAPs associated with structural and functional defects of the ventral disc

Our lab recently developed CRISPR-Cas9-mediated transcriptional KD (CRISPRi) for *G. lamblia* (McInally et al., 2019a,b), enabling genetic analyses of the many unique disc proteins and protein complexes. Using morpholino or CRISPRi-mediated KD, we previously observed dramatic defects in the disc that highlight the structural and functional roles of the disc-associated median body protein (MBP) (Woessner and Dawson, 2012; McInally et al., 2019a,b). Here, we screened 14 CRISPRi KD strains to evaluate the contributions of specific DAPs to stabilizing the disc or limiting disc MT dynamics. These DAPs were chosen based on their limited and representative localizations to one of the disc regions defined in Figs 2,3. CRISPRi KD was performed in the mNGβtubNeo background strain, which contains a single integrated copy of mNeonGreen-tagged β-tubulin to allow easy visualization of disc MT defects. Initial visual screening and hyperstability assays indicated that 13 KD strains (all but DAP5188+288R) had discs with a wild-type appearance and 12 strains (all but DAP5188+288R and DAP6751+17R) had discs that retained wild-type stability. The 12 DAP KD strains in this initial screen with wild-type appearing, hyperstable discs were excluded from further analysis for this study (DAP3951+17R, DAP4410+618R, DAP5489+23R, DAP5883+62R, DAP9515+11R, DAP11554+17R, DAP16263+48R, DAP16342+44R, DAP17053+65R, DAP17551+11R, DAP23492+15R and DAP40016+30R). Two remaining KD strains (DAP5188+288R and DAP6751+17R) were examined further (see Fig. 2B and Fig. S4). Knockdown of DAP5188, an ankyrin-repeat protein, in the mNGβtubNeo background strain resulted in discs with an open, flattened conformation with less overall tubulin localization than the mNGβtubNeo non-specific gRNA (nsgRNA) strain (Fig. 4A–C). Population-level quantitative reverse transcription (qRT)-PCR of three independent electroporations of the DAP5188+288R strain indicated an average of ∼47% KD of DAP5188 transcription (normalized to

Journal of Cell Science (2020) 133, jcs227355. doi:10.1242/jcs.227355

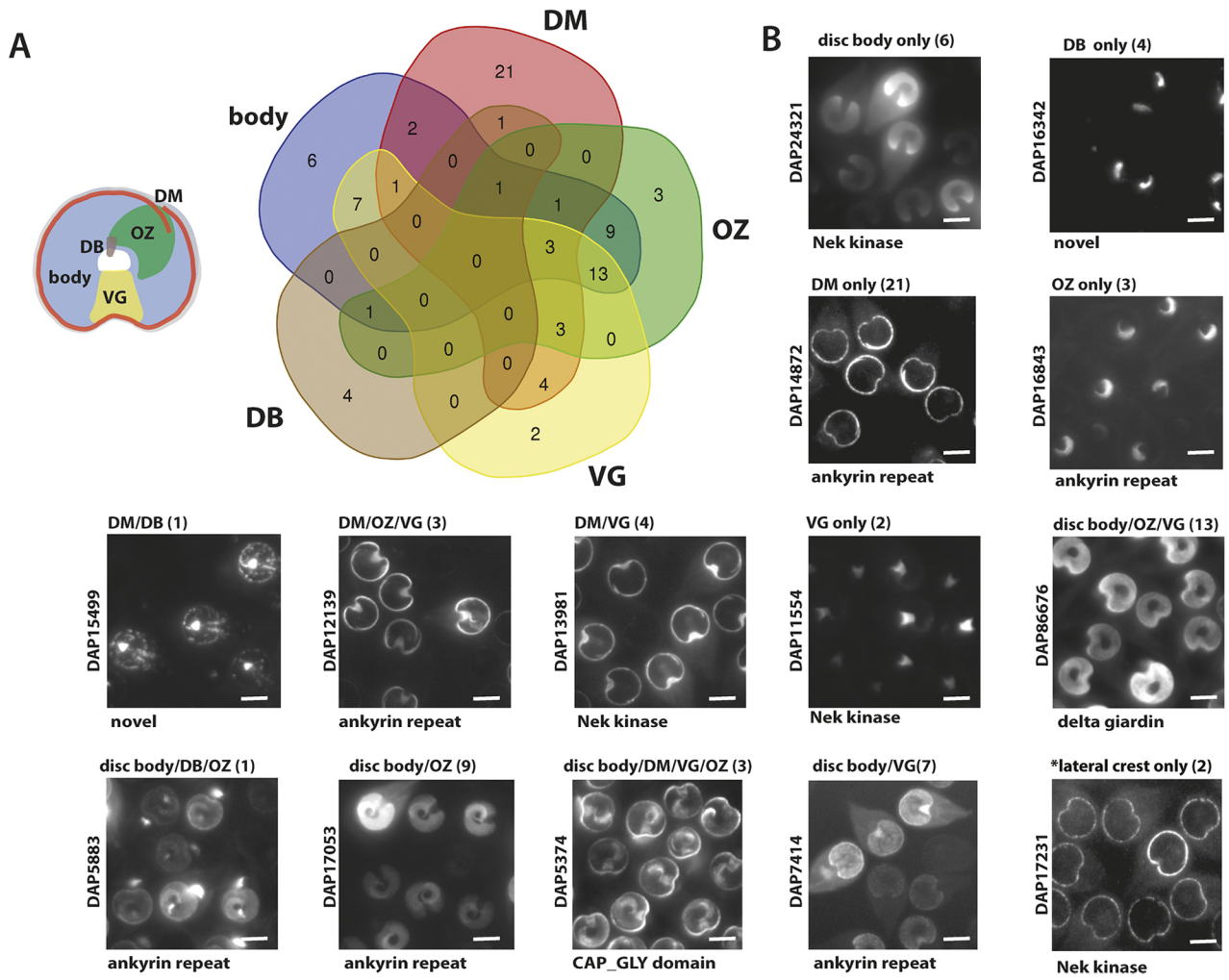

Fig. 3. DAPs localize to structurally distinct regions of the ventral disc. (A) Venn diagram showing the categorization of DAPs by their localization to distinct regions of the disc, including the MT spiral array (body), disc margin (DM), ventral groove (VG), dense bands (DB) and overlap zone (OZ). (B) Shown are 14 representative DAPs that define each of the localization categories. Whereas a representative lateral crest image is included, the last image (*) indicates that – in order to simplify the representation – six DAPs with lateral crest localization were not included in the Venn diagram. Also omitted was a representative image for the disc body/lateral crest category. Scale bars: 5 µm.

GAPDH expression) as compared to the average, normalized DAP5188 expression in three independent non-specific guide (nsgRNA) strains (Fig. 4D). Immunostaining of the DAP5188KD strain with anti-Cas9 antibody showed that the catalytically inactive Cas9 variant (dCas9) localized to the nuclei of ∼25% of the trophozoites in the population (Fig. 4E). Nearly 15% of all cells in the DAP5188KD population had ventral disc defects as compared to the nsgRNA strain, yet aberrant disc phenotypes were >40% penetrant when correlated with dCas9-positive cells (Fig. 4F), supporting the population-level estimates of overall decreased DAP5188 expression observed using qRT-PCR (Fig. 4C). Knockdown of DAP6751, a novel protein, did not result in obvious visual structural defects (Fig. 4B), thus the aberrant disc phenotypic penetrance was not significantly higher than any disc phenotypic variance in the nsgRNA strain. Using qRT-PCR of three independent electroporations of the DAP6751+17R strain, we found an average KD of ∼23% of DAP6751 expression (normalized to GAPDH expression) as compared to DAP6751 normalized expression in three independent non-specific guide (nsgRNA) strains. dCas9 was also detected in the nuclei of ∼25% of the DAP6751KD strain population.

Ventral discs in the DAP5188 KD strain are sensitive to drugs that limit MT dynamics

We have previously shown that, in interphase, the ventral disc is insensitive to drugs that limit MT dynamics (Dawson et al., 2007), yet the MTs of the eight flagella, median body and mitotic spindles are sensitive to MT drugs (Dawson et al., 2007). Here, we developed quantitative imaging assays to evaluate the sensitivity of the MT organelles of CRISPRi KD strains to drugs that stabilize or inhibit MT polymerization (Fig. 5). After separate treatments of trophozoites with Taxol or nocodazole, we quantified the area and overall structure of the disc body, overlap zone and central bare area. As we have previously reported, the area and conformation of the ventral disc are unaffected by treatment with MT drugs (Fig. 5A,B); however, the MTs of other MT organelles (e.g. the flagella or median body) were sensitive to these MT drugs as indicated by differences in the sizes of these organelles following drug treatments (Fig. 5C).

DAP5188 localized to the disc body, disc margin, overlap zone and ventral groove (Fig. 4 and Fig. S4). To evaluate the effects of MT drugs after DAP5188 KD, the DAP5188KD and nsgRNA

Journal of Cell Science (2020) 133, jcs227355. doi:10.1242/jcs.227355

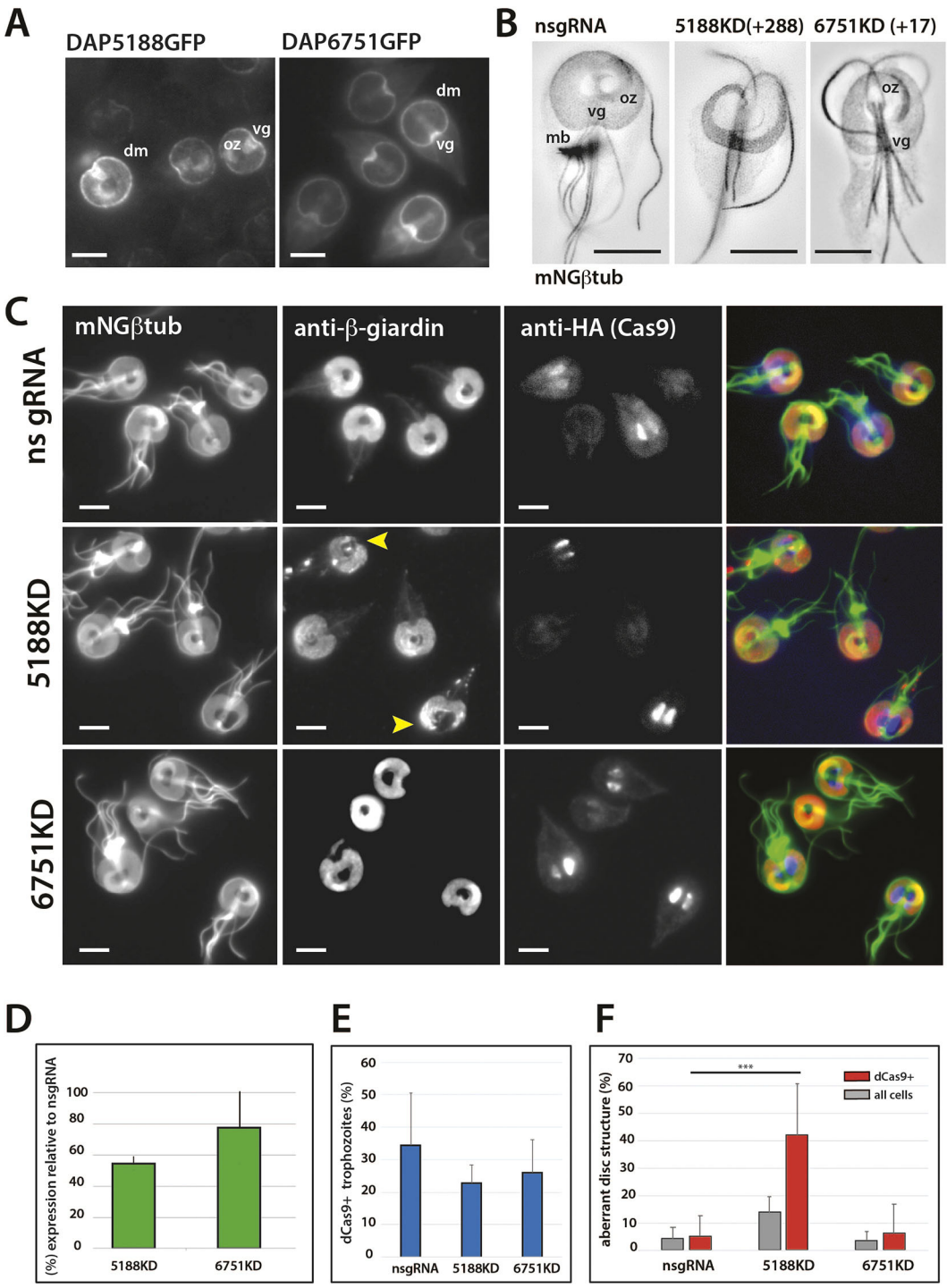

Fig. 4. Stable CRISPRi-mediated knockdowns of the disc margin proteins DAP5188 and DAP6751 have structural defects in the ventral disc. (A) C-terminal GFP fusions of the ankyrin-repeat domain protein DAP5188 and the newly identified protein DAP6751 localize to the disc margin (dm) and ventral groove (vg) regions of the ventral disc. DAP5188GFP also localizes to the disc body and overlap zone (oz). (B) High resolution SIM images of the cytoskeletal structure after CRISPRi-mediated KD of DAP5188 and DAP6751 in the mNGβtubNeo strain (inverted grayscale). (C) CRISPRi KDs of DAP5188 and DAP6751 (5188KD and 6751KD, respectively) in the mNGβtubNeo strain, immunostained with antibodies against β-giardin (microribbons) and HA (3×HA-tagged dCas9). (D) Quantification of the average expression of DAP5188 and DAP6751, normalized to the average expression of GAPDH in each strain. Error bars indicate +s.e. and correspond to the three independent electroporations of each strain. (E,F) Quantification of dCas9, as well as the penetrance of the aberrant disc phenotype within single cells. Aberrant discs in both the DAP5188KD(+288) and DAP6751KD(+17) strains are correlated with the presence of dCas9 nuclear staining, as compared to the nsgRNA control (see arrows in C). The normalized average expression of DAP5188 and DAP6751 in the KD strains is presented as a percentage of DAP5188 or DAP6751 normalized expression in the non-specific gRNA (nsgRNA) strain. dCas9 penetrance was quantified for the three independent electroporations of CRISPRi in both DAP KD strains. Of cells in each CRISPRi strain, ∼25% express dCas9 (E), and aberrant disc phenotypes are strongly correlated with dCas9 expression (F) for the DAP5188KD (n=311) as compared to the nsgRNA strain (n=282). Few aberrant discs were visually observed for the DAP6751KD strain (n=148), such that a similar phenotypic correlation with dCas9 presence was not possible. In E and F, means and the corresponding confidence intervals (mean±c.i.) are presented for each experimental condition. Statistical significance was assessed using the unpaired t-test with ***$P\leq0.05$. Scale bars: 5 µm.

Journal of Cell Science (2020) 133, jcs227355. doi:10.1242/jcs.227355

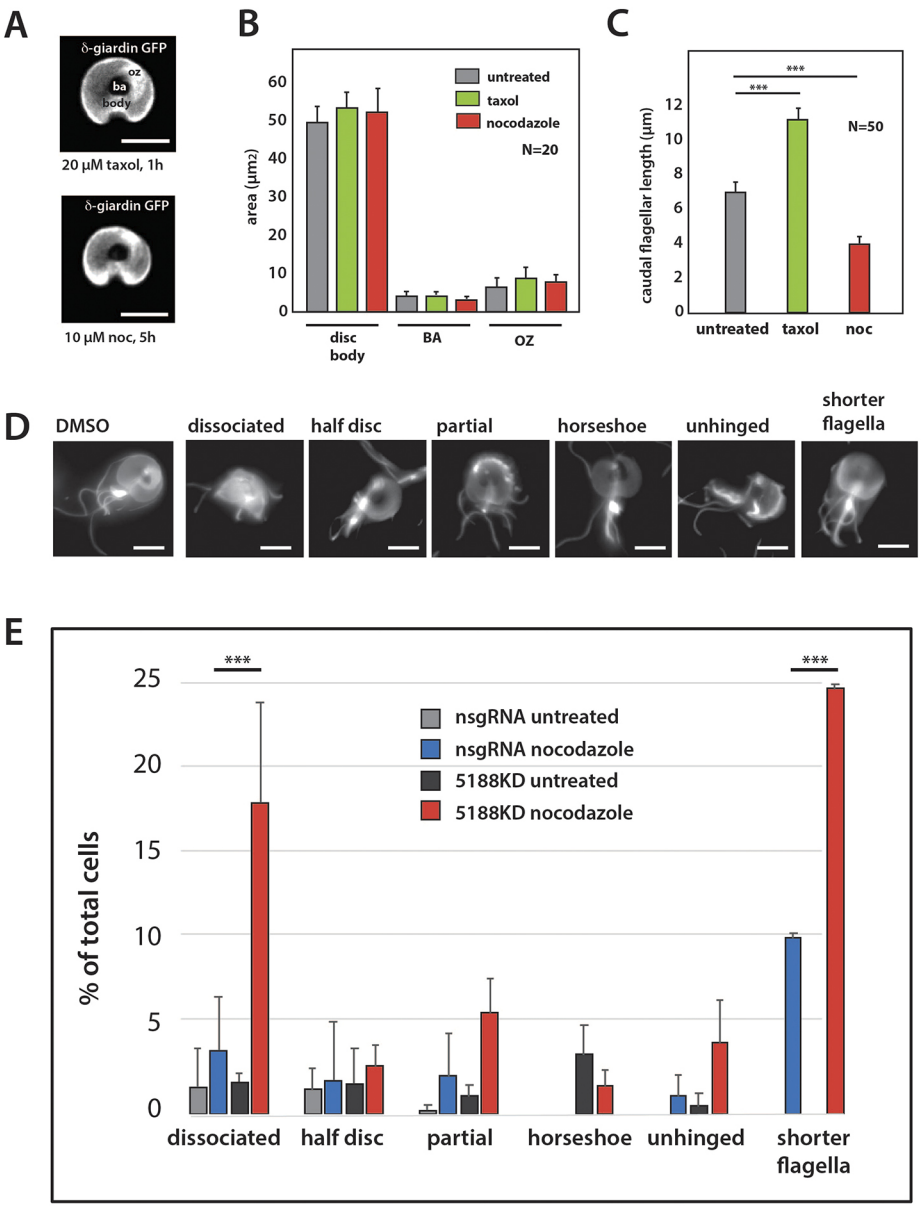

Fig. 5. Disc MT disassembly is increased in the DAP5188KD strain after nocodazole treatment. Trophozoite interphase MT dynamics are normally limited to the flagellar tips and the median body (Dawson et al., 2007). (A,B) Quantification of the effects of MT drugs on the area and overall structure of the disc body (body), overlap zone (oz) and central bare area (ba) in live cells following treatment with 10 µM nocodazole (5 h) or 20 µM Taxol (1 h). (C) Under the same treatment conditions, the eight flagella are sensitive to MT drugs and either lengthen (Taxol) or shorten (nocodazole). (D,E) Ventral discs of the DAP5188KD strain are sensitive to treatment with 10 µM nocodazole. Nocodazole treatment resulted in five distinct disc disassembly categories that were scored in fixed trophozoites (representative images are shown in D). (E) Discs in nocodazole-treated DAP5188KD cells (n=119) and untreated DAP5188KD DMSO vehicle control cells (n=127) were scored, and compared to treated (n=106) and untreated nsgRNA strain controls (n=135). Flagellar lengths were also more sensitive to length dynamics in the DAP5188KD strain (shorter flagella category). Means are presented with corresponding confidence intervals (mean±c.i.) for biological replicates of each experimental condition. Significance was assessed using the unpaired t-test with ***P≤0.05. Scale bars: 5 µm.

strains were each treated with nocodazole, and control cells were incubated with DMSO. Cells were then fixed and imaged by light microscopy, and ventral disc structural phenotypes were scored. In contrast to the nsgRNA strain, nocodazole treatment of the DAP5188KD strain resulted in an enrichment of five distinct phenotypic classes associated with increased levels of MT depolymerization in the disc (Fig. 5D). These MT drug-sensitive phenotypes included ‘dissociated’, in which the disc was largely disassembled; ‘half disc’, in which 50% of the disc was present; ‘partial’, in which the disc spiral was disrupted but the overlap zone was left intact; ‘horseshoe’, with an opened and flattened disc lacking an overlap zone; and ‘unhinged’, typified by a disc lacking an overlap zone, allowing the two ends of the disc spiral to rotate freely. We also determined the proportion of cells with ‘shorter flagella’, which was scored separately from the five categories described above. More than 25% of nocodazole-treated DAP5188KD trophozoites had a scorable phenotype, with the majority having dissociated (18%) or partial (~6%) disc phenotypes. Other scorable phenotypes (e.g. half disc, horseshoe and unhinged) were present but less abundant in the population of nocodazole-treated cells (Fig. 5E). Only ~5% of the untreated DAP5188KD (DMSO only) control trophozoites had scorable phenotypes. Furthermore, after nocodazole treatment, cells with shorter flagella were at least twice as abundant in the DAP5188KD strain as in the nsgRNA strain (Fig. 5E).

CRISPRi-mediated KD of the ankyrin-repeat protein DAP5188 or the novel protein DAP6751 limits hyperstable properties of the disc

To determine whether DAPs are required to maintain the hyperstable properties of the core disc ultrastructure, we adapted the biochemical fractionation protocol used to identify new disc proteins as an assay for disc integrity in various DAP KD strains. Whole intact discs were first extracted from cells using PHEM with detergent and a high-salt concentration (2 M KCl) indicating that the disc is ‘hyperstable’. Increased salt concentration had little effect on the dissociation of DAPs – as indicated by SDS-PAGE (Fig. 6A); and GFP-tagged disc proteins, such as DAP16343 (MBP), remain

Journal of Cell Science (2020) 133, jcs227355. doi:10.1242/jcs.227355

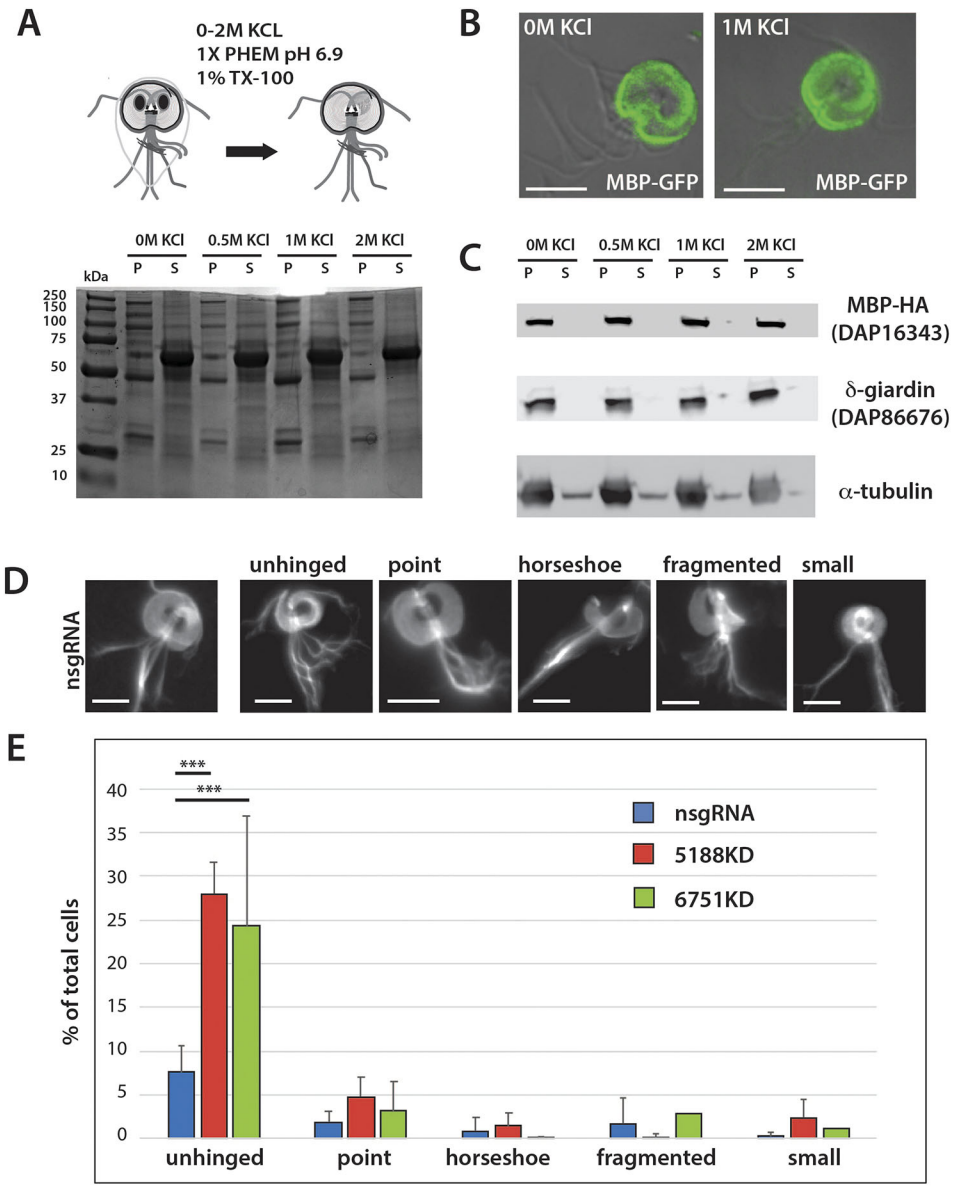

Fig. 6. Ventral discs from DAP5188KD and DAP6751KD strains dissociate after fractionation with high-salt and detergent. (A) SDS-PAGE of fractions (pellet P1 and supernatant S1) from extractions with 0–2 M KCl indicating that increased concentrations of KCl have little effect on the distribution of proteins from the fractionated discs. (B) In support, the GFP-tagged disc protein MBP (green) remains fluorescent and associated with the disc, even after extraction with 1 M KCl. (C) Western blot analysis of the SDS-PAGE shown in A, showing that α-tubulin, the MR protein δ-giardin (DAP86676), and HA-tagged MBP (DAP16343) (Woessner and Dawson, 2012) remain associated with the pelleted fraction regardless of the salt concentration (0–2 M KCl). Five categories of disc-dissociation phenotypes are observed in DAP5188KD and DAP6751KD strains after treatment. (D) Representative disc-dissociation categories are shown for the DAP5188KD strain; similar categories were observed and scored for the DAP6751KD strain (see Materials and Methods). (E) Disc-dissociation phenotypes were ranked and quantified for extracted discs from each of the three independent electroporations of the nsgRNA (blue; *n*=342), DAP5188KD (red; *n*=348) and DAP6751KD (green; *n*=635) strains. Means are presented with corresponding confidence intervals (mean ±c.i.) for biological replicates of each experimental condition. Significance was assessed using the unpaired *t*-test with ***$P \leq 0.05$. Scale bars: 5 µm.

associated with the disc even after extraction with 2 M KCl (Fig. 6B). α-tubulin and δ-giardin (a component of the MRs) also remain associated with the disc following high-salt extraction (Fig. 6C).

Stability and integrity of discs in the two CRISPRi KD strains were also evaluated following high-salt and detergent extraction (Fig. S1). Discs from the mNGβtubNeo strain retain fluorescence after extraction, allowing straightforward visual phenotypic scoring of hundreds of extracted discs. In both the CRISPRi DAP5188KD and DAP6751KD strains, we categorized five distinct phenotypic classes on the basis of severity of disc structural defects observed following disc fractionation with 2 M KCl. The least severe was ‘fragmented’, typified by an intact overlap zone and fully enclosed bare area, with disruption to small parts of the disc. This was followed by ‘point’, which lacked most of the overlap zone but retained enough to hold the two ends of the disc spiral together; ‘unhinged’, with flattened, open discs that lacked an overlap zone but appeared to have the same tubulin content as wild-type discs; and ‘horseshoe’, characterized by flattened open discs that lacked an overlap and had less tubulin than the unhinged phenotype. The most severe phenotype was ‘small’, in which only the central region of disc was maintained (Fig. 6D). As compared to the nsgRNA strain, >30% of CRISPRi 5188KD trophozoites had a scorable phenotype, with <30% of discs having an ‘unhinged’ disc phenotype (Fig. 6E). Other less-abundant phenotypic categories were ‘point’ or ‘small’. Of CRISPRi DAP6751KD discs, ∼30% also had an aberrant phenotype following high-salt extraction. Phenotypes of the DAP6751KD strain were less severe, yet ∼25% of discs had an ‘unhinged’ structure after high-salt extraction; ∼5% of the DAP6751KD disc phenotypes included other categories, such as ‘point’ or ‘fragmented’.

DISCUSSION

Cytoskeletal innovation is widespread in eukaryotic cells (Dawson and Paredez, 2013) and the elaborate architecture of the ventral disc in *G. lamblia* highlights the unique functional properties of diverse MT organelles (Russell et al., 2017). Ventral disc MTs scaffold the numerous novel and repetitive protein densities that make up the complex disc ultrastructure (Brown et al., 2016; Cheissin, 1964; Schwartz et al., 2012); however, the protein composition and

Journal of Cell Science (2020) 133, jcs227355. doi:10.1242/jcs.227355

functional roles of the repetitive MT-binding complexes governing the stability and functioning of the disc are not well understood.

By using a modified biochemical extraction protocol with shotgun proteomic analyses, combined with an ongoing subcellular localization screen, we identified and confirmed 53 new disc-associated proteins (DAPs) (Fig. 2), bringing the known DAPs to 87 in total. This study nearly triples the number of previously described DAPs (Hagen et al., 2011; Lourenço et al., 2012). Twenty-seven new DAPs are present in the detergent-extracted disc proteome, whereas the additional 26 identified by localization alone were below a threshold abundance of at least five peptides in the proteomic analyses (Table S2). Of the 87 DAPs, 85 lack similarity to known MT-associated proteins (Fig. 2) and close to one-third lack any similarity to proteins outside of *Giardia* species (Andersson et al., 2007).

Our subcellular localization of the 87 DAPs defined strikingly varied, yet distinct, localization patterns (Figs S2 and S3) that mirror the structural regions in the disc recently defined by cryo-ET (Brown et al., 2016). Specific DAPs localize to the disc margin, the dense bands, ventral groove and overlap zone regions, or the entire disc body (Fig. 3 and Figs S2–S5). DAPs associated with particular regions of the disc MT structure might, therefore, confer specific structural or functional properties (e.g. limited MT dynamics or hyperstability) that define particular regions of the disc architecture.

A new role for DAPs in limiting disc MT dynamics during interphase

Like other protists, *G. lamblia* simultaneously modulates the dynamics and stability of its MT organelles during interphase, cell division and encystation and/or excystation (Dawson et al., 2007). Although the two spindles, median body and eight flagella of *G. lamblia* exhibit both interphase and mitotic MT dynamics, such dynamics are severely limited in the interphase disc (Dawson et al., 2007; Fig. 5). Singlet MTs, such as those that comprise the mitotic spindle, typically exhibit dynamic instability – the property of MT plus ends to stochastically switch between growing and shrinking states (Mitchison and Kirschner, 1984). Dynamic instability can be stabilized or modulated by the activities of various MT plus-end-binding proteins (e.g. EB1, XMAP215) (Akhmanova and Steinmetz, 2015; Bowne-Anderson et al., 2015). Such MT plus-end-tracking proteins (+TIPs) accumulate at growing MT plus ends, where they modulate and couple dynamic MT movements to cellular structures (Akhmanova and Hoogenraad, 2005).

Here, we identified 38 DAPs that localize to the disc margin, i.e. the region of the disc that is the primary location of the MT plus ends (Brown et al., 2016). The majority of disc margin-localizing DAPs have ankyrin-repeat domains (15 DAPs) or NEK domains (six DAPs) but ten disc margin DAPs lack similarity to any known protein. Twenty-one DAPs localize exclusively to this region (Fig. 3 and Fig. S3), yet we have not identified *G. lamblia* homologs of conserved plus-end-binding proteins like EB1 (Dawson et al., 2007) or XMAP215 at the disc margin. Other MT plus ends are present in the terminal edge of the overlap zone region, to which 34 DAPs also localize. The majority of these ‘overlap zone’ DAPs also localize to the disc margin or disc body (Fig. S5).

The genetic interrogation of protein function in *G. lamblia* has been generally limited due to a lack of robust genetic tools and the presence of two diploid nuclei. Our recent adaptation of CRISPR interference (CRISPRi) in *G. lamblia* allows for the rapid evaluation of loss-of-function phenotypes (McInally et al., 2019a,b). CRISPRi employs the catalytically inactive Cas9 variant dCas9 to block transcription and/or elongation, resulting in stable, inducible or reversible gene KD in eukaryotes (Larson et al., 2013; Piatek et al., 2015) or bacteria (Kaczmarzyk et al., 2018; Larson et al., 2013; Liu et al., 2017; Tao et al., 2017; Zhang et al., 2016; Zuberi et al., 2017). Precise targeting is achieved using a complementary guide RNA to direct the inactive dCas9 to a specific genomic locus. CRISPRi is an effective alternative to RNAi transcriptional silencing in many systems and has been shown to have significantly fewer off-target effects (Larson et al., 2013; Smith et al., 2017; Stojic et al., 2018). Our recent demonstration of CRISPRi in *G. lamblia* showed that we could stably KD the transcription of endogenous and exogenously expressed proteins (McInally et al., 2019a,b). The *G. lamblia* CRISPRi KD plasmid can be electroporated into an existing strain that has an integrated subcellular marker, such as the mNGβtubNeo strain used here to screen and visualize defects in disc, flagellar or median body organization.

One possible role for the newly described disc margin and overlap zone DAPs is to specifically limit dynamic instability at the plus ends of ventral disc MTs in these regions, resulting in the stable interphase disc structure that is insensitive to nocodazole or Taxol (Fig. 5A). To test this idea, we created and screened several CRISPRi-mediated KDs of disc margin DAPs and determined that one, DAP5188, has a significant impact in limiting MT dynamics in the disc during interphase (Fig. 5). DAP5188 localizes to the disc margin as well as the overlap zone, disc body and ventral groove region (Fig. 4, Fig. S4 and Table S2), and is one of 32 DAPs with at least one ankyrin-repeat domain (Fig. 2B, Table S2). Structurally, DAP5188 is defined by one N-terminal and one C-terminal ankyrin repeat. Knockdown of DAP5188 results in discs with an open flattened disc conformation (Fig. 4). We have previously shown similar phenotypes with morpholino or CRISPRi-based KDs of the overlap zone protein DAP16343 (or median body protein), which results in discs with flattened open conformations and parasites with significant attachment defects (McInally et al., 2019a,b; Nosala et al., 2018; Woessner and Dawson, 2012). Many *G. lamblia* proteins that we identified in this or previous studies localize to disc regions with known MT plus-end termini (Brown et al., 2016) and might play a similar role in MT plus-end binding or in modulating plus-end dynamics in the disc.

Nocodazole-induced inhibition of MT polymerization has been used widely as an indication of high-affinity MT binding (Hoebeke et al., 1976). Nocodazole binds free tubulin dimers, preventing their incorporation into growing plus ends of MTs. During nocodazole treatment, MT-binding proteins stabilize MT dynamics at the MT plus ends, thus protecting growing MTs from steady-state cellular processes favoring MT depolymerization. Here, we defined a cellular role for DAP5188 in stabilizing disc MT dynamics. Unlike wild-type discs that are insensitive to MT drugs (Fig. 5A,B), discs in the DAP5188KD strain are sensitive to nocodazole (Fig. 5D,E). Following nocodazole treatment, discs in the DAP5188KD strain were partially to almost completely disassembled (Fig. 5D).

Stable interphase lengths of each of the four *G. lamblia* flagellar pairs were maintained through assembly by intraflagellar transport (IFT) mechanisms, counterbalanced by disassembly mechanisms mediated at flagellar tips by the depolymerizing MT motor kinesin-13 (Dawson et al., 2007; McInally et al., 2019a,b). Nocodazole treatment generally limits MT assembly and, thus, shifts the balance towards MT disassembly at flagellar tips, resulting in shorter flagella (Fig. 5C; see also Dawson et al., 2007; McInally et al., 2019a,b). Here, we observed that nocodazole treatment doubled the number of shortened flagella in the DAP5188KD strain as compared to the nocodazole-treated nsgRNA control strain

Journal of Cell Science (2020) 133, jcs227355. doi:10.1242/jcs.227355

(Fig. 5D,E). We interpret this difference as the loss of MT-stabilizing DAP5188 in KD mutants, causing flagellar tips MT to become more susceptible to the activity of constitutive MT-depolymerizing proteins, such as kinesin-13 (Dawson et al., 2007; McInally et al., 2019a,b). This increased susceptibility of flagella to MT depolymerization might, thereby, result in the increased number of trophozoites with shorter flagella lengths. Therefore, we suggest that DAP5188 acts as a more-general plus-end-binding protein, stabilizing both the disc and flagellar MT plus ends by limiting MT depolymerization during interphase.

A functional role for an ankyrin-repeat protein in selectively stabilizing MT plus ends has not been identified previously; however, a synthetically designed ankyrin-repeat protein (DARPin) that interferes with MT assembly by binding to exposed MT plus ends has been created (Pecqueur et al., 2012). Whereas ankyrin repeat proteins generally mediate protein–protein interactions and protein stability (Li et al., 2006), some ankyrin proteins have been shown to interact directly or indirectly with MTs. For example, ankyrin proteins found in human erythrocytes, muscles and neurons stabilize subsets of MTs, and can directly interact with tubulin *in vitro* (Bennett and Davis, 1981; Davis and Bennett, 1984). Furthermore, in the elaborate conoid MT organelle of the apicomplexan protist *Toxoplasma gondii*, an ankyrin-repeat protein (CPH1) links structural and motor proteins, and may interact with the tubulin-rich conoid fibers (Long et al., 2017). Whether other disc margin or overlap zone DAPs have similar properties in limiting assembly at the plus ends of disc MTs remains to be determined. The abundance of ankyrin-repeat proteins localized to the disc suggests that *G. lamblia* ankyrin-repeat proteins play similar and essential roles in limiting disc MT dynamics or stability.

The specific mechanism by which the ankyrin-repeat protein DAP5188 stabilizes MTs may also offer insight into the mechanisms of drug resistance to the benzimidazole class of compounds used to treat giardiasis, including both nocodazole and albendazole (Lindquist, 1996; Upcroft et al., 1996). Nocodazole and other benzimidazoles are potent inhibitors of cell division in *G. lamblia* and might also limit disc-mediated attachment to the host intestinal epithelium (Morgan et al., 1993). Albendazole resistance has been reported in *G. lamblia*, yet the mechanism of resistance is unknown. Albendazole resistance in helminths has been correlated to mutations in β-tubulin, yet similar mutations in *G. lamblia* β-tubulin are not associated with albendazole resistance (Lindquist, 1996; Upcroft et al., 1996). Resistant strains possess aberrant MT structures, including enlarged median bodies (Upcroft et al., 1996) indicative of unregulated MT dynamics. Thus, rather than β-tubulin mutations, it is possible that the reported resistance to commonly used benzimidazoles in *G. lamblia* is associated with mutations in MT-associated proteins, particularly those that modulate the affinity or activity of DAPs that limit MT dynamics, such as DAP5188.

DAPs are important for the hyperstability of the ventral disc

The singlet MTs of the curved, domed disc spiral array must withstand intense mechanical forces – much like the mechanical forces acting on axonemal doublet MTs during ciliary beating (Linck et al., 2014). The hyperstability of cilia, centrioles and basal bodies is thought to derive from the overall stabilizing ultrastructure of the doublet and triplet MTs (Linck et al., 2014), as well as from MAPs binding to the outside of protofilaments. MIPs form a scaffold inside the lumen of ciliary MTs, possibly enabling both MT stability and flexibility (Ichikawa and Bui, 2018). Various post-translational modifications of tubulin (PTMs) also directly or indirectly influence MT stability by regulating the localization of MAPs or other proteins that affect MT dynamics in various MT organelles (Garnham and Roll-Mecak, 2012). In contrast to cilia, the ventral disc is composed of singlet, not doublet, MTs and, thus, the disc MT ultrastructure alone is not sufficient for MT stability.

How, then, is hyperstability of the singlet disc MTs achieved? Almost all protofilaments of the disc MTs are coated with regularly spaced DAPs and higher order structures, such as the MR–CB complex (Fig. 1) (Brown et al., 2016). MR–CB complexes (Fig. 1) in particular have been implicated in the stabilization of the domed disc conformation (Holberton and Ward, 1981; Nosala et al., 2018). Three MR DAPs are SF-assemblin homologs, which stabilize both ciliary root structures in ciliated protists (Nabi et al., 2019; Weber et al., 1993) and MTs of the *Toxoplasma* apical complex (Francia et al., 2012). It is reasonable to suspect that disc hyperstability is mediated not only by MRs, but also through the other DAPs closely associated with the disc MTs.

G. lamblia lacks homologs of many canonical MAPs, such as tektin or tau, which are known to stabilize MTs (Amos, 2004, 2008; Morrison et al., 2007). To evaluate the roles of the many novel or ankyrin-repeat DAPs in *G. lamblia* that stabilize the disc architecture, we tested the integrity of discs in 14 CRISPRi DAP KD strains following high-salt and detergent extraction (Fig. 6A,B) (Crossley and Holberton, 1983b; Holberton and Ward, 1981). In contrast to discs from a nsgRNA control strain, we identified two DAP CRISPRi-mediated KD strains – DAP5188KD and DAP6751KD – whose discs were destabilized or dissociated following high-salt fractionation (Fig. 6D,E). Thus, DAP5188 and DAP6751 help to mediate hyperstability through direct or indirect interactions with the disc MTs. Discs from the DAP5188KD strain showed even greater dissociation following extraction than discs from the DAP6751KD strain (Fig. 6E). Because DAP6751 lacks similarity to other proteins, the mechanism by which DAP6751 helps to stabilize the disc remains unclear; however, the localization of both DAP6751 and DAP5188 to the disc margin could imply that the stabilization of the disc periphery is necessary to limit overall destabilization of the disc during fractionation as previously proposed (Holberton, 1981).

Conserved MIPs might also contribute to disc stability and flexibility

In addition to outer binding MAPs, an inner luminal scaffold formed by MIPs in MTs is thought to strengthen tubulin dimer and protofilament coherence, and promote MT stability and/or elasticity during ciliary beating to limit MT breakage (Ichikawa and Bui, 2018). MIPs also stabilize the singlet subpellicular MTs of the malarial parasite *Plasmodium*, enabling the stable, yet highly elastic, sporozoite cytoskeleton to flex as the parasites squeeze through host tissues (Cyrklaff et al., 2007). The three MIPs (gMIPs) that periodically repeat in the lumen of the disc singlet MTs might also support the structural integrity and extreme stability of the disc (Schwartz et al., 2012). Although the molecular identities of gMIPs remain unknown, we confirmed that DAP41512 – a Rib72 homolog with a DUF1126 domain – localizes to the disc margin, flagella and median body (Figs 2, 3; Fig. S3). Rib72 homologs may be globular MIPs, and *Tetrahymena* RIB72A and RIB72B are essential for the assembly of A-tubule MIPs in cilia (Stoddard et al., 2018). FAP52 is another widely conserved MIP that has recently been shown to localize to the inner junction of doublet MTs (Owa et al., 2018). The two FAP52 homologs (DAP15218 and DAP15956) in *G. lamblia* also localize to the stable singlet MTs of the disc and median body, as well as to the doublet axonemal MTs (Fig. 2). These localizations

Journal of Cell Science (2020) 133, jcs227355. doi:10.1242/jcs.227355

of *G. lamblia* Rib72 and FAP52 MIP homologs to the stable singlet MTs of the disc, and to the more-dynamic median body MTs support a more-general role for MIPs in promoting the stability and elasticity of interphase singlet MTs, in addition to stabilizing doublet and triplet MTs in axonemes. Moreover, two newly identified DAPs (DAP9148 and DAP103164) that localize to both the disc and axonemes (Fig. 3 and Table S2) are homologous to SHIPPO-repeat domain proteins. Although not studied outside of metazoans, SHIPPO-repeat proteins have been predicted to stabilize and add rigidity to MTs of the mammalian sperm tail (Egydio de Carvalho et al., 2002).

Additional functions of DAPs in promoting disc assembly, MT nucleation or parasite attachment to the host epithelium

Disc MTs are thought to nucleate primarily at a series of perpendicular bands termed the dense-band nucleation zone, as disc MT minus ends do not directly contact the basal bodies (Brown et al., 2016). The three distinct dense bands comprise two regions of tightly packed MTs that spiral into the nearly flat single plane at the base of the spiral disc MT array. Although we have now identified six DAPs localizing to the dense-band region (Fig. 3), the mechanism by which the dense bands support MT nucleation is unknown. Additionally, novel DAPs could mediate MT nucleation in the disc margin, as ∼39% of disc MTs nucleate from this region, possibly through a branching nucleation-type mechanism (Brown et al., 2016).

Disc-associated proteins, like DAP5188 or DAP6751, might also regulate dorsal daughter disc assembly and parental disassembly during division and encystation, resulting in the observed aberrant disc structural or stability phenotypes. During the rapid mitosis and cytokinesis of *G. lamblia* (Hardin et al., 2017), two daughter discs are assembled *de novo* on the anterior dorsal side of the parent cell, with the ventral sides of the new discs exposed on the cell surface (Tůmová et al., 2007). Other DAPs may also contribute to disc assembly. *G. lamblia* has an expanded repertoire of >70 NIMA-related kinases (or NEKs) (Manning et al., 2011) and 13 NEKs localize to various regions of the disc (Table S2). Members of the NEK family regulate centrosome separation, spindle assembly and cytokinesis during cell division through targeted phosphorylation of proteins associated with the MT cytoskeleton (Fry et al., 2017). Two disc NEKs are putatively cell cycle-specific (Davids et al., 2011). In addition to putative regulatory roles, the disc associated NEKs may contribute to disc architecture and stability or even to attachment dynamics.

Some of the newly identified DAPs might have less obvious roles in disc architecture, hyperstability, or MT dynamics. Presumably, DAPs are also required for the generation of forces by the disc for attachment to the host. DAPs could contribute to facilitating curvature and doming of the disc, or to regulating the functional properties of the disc necessary for attachment. We anticipate that the ongoing use of newly developed genetic tools, such as CRISPR interference (CRISPRi), to repress both single or multiple endogenous genes in *G. lamblia* (McInally et al., 2019a,b) will continue to uncover unique functions of DAPs regarding disc architecture, stability and flexibility during attachment-mediated infection in this widespread parasite.

MATERIALS AND METHODS

Strains and culture conditions

The *Giardia lamblia* strain WBC6 (ATCC 50803) was used to construct the DAP-GFP strains and the mNGβtubNeo background strain for CRISPRi KD s. All KD or control strains were routinely cultured in sterile 16 ml screw-capped disposable tubes (BD Falcon) containing 12 ml modified TYI-S-33 medium supplemented with bovine bile and 5% adult bovine serum and 5% fetal bovine serum (House et al., 2011). Cultures were incubated upright at 37°C without shaking and screened regularly for bacterial contamination. Puromycin was added to culture medium at a final concentration of 50 µg/ml to select for episomal plasmids in GFP and CRISPRi KD strains.

C-terminal GFP tagging of candidate disc-associated proteins

The construction of the median body protein (MBP)-GFP strain used to assess detergent extraction and dissociation of the disc with increasing KCl concentrations was described previously (Woessner and Dawson, 2012). All other *G. lamblia* DAP-GFP strains were created using Gateway cloning as previously described (Hagen et al., 2011). To add C-terminal GFP fusion tags to candidate DAPs, PCR forward primers were designed to bind 200 bp upstream of the gene to include the *G. lamblia* native promoter. Full-length genes lacking stop codons were amplified from *G. lamblia* strain WBC6 genomic DNA using either PfuTurbo Hotstart PCR Master Mix or Easy-A High Fidelity PCR Master Mix (Agilent) and were cloned into the Thermo Fisher Scientific Gateway entry vectors pENTR/D-TOPO (for blunt-end, directional TOPO cloning) or pCR8/GW/TOPO (for efficient TOPO TA cloning), respectively. Inserts were sequenced to confirm gene identity and correct orientation. To generate DAP-GFP fusions, entry vectors were recombined with the *E. coli* and *G. lamblia* Gateway destination vector pcGFP1Fpac (GenBank #MH048881) (Dawson and House, 2010) through LR recombination by using LR Clonase II Plus (Thermo Fisher Scientific). Clones were screened by AscI digest and the Plasmid Plus Midi Kit (Qiagen) was used to prepare bulk plasmid DNA. To create *G. lamblia* strains that express GFP-tagged candidate DAPs, plasmid DNA (20 µg) was introduced into 1×10^7 *G. lamblia* strain WBC6 (ATCC 50803) trophozoites by electroporation using a Bio-Rad GenePulserXcell as previously described (Dawson et al., 2007). Transfectants were initially selected with 10 µg/ml puromycin; the antibiotic concentration was increased to 50 µg/ml once cultures reached 50% confluence (typically 7–10 d). Cultures were maintained with selection for at least two weeks prior to the preparation of frozen stocks.

Construction of the *G. lamblia* mNGβtubNeo background strain for CRISPRi KDs

To generate *G. lamblia* strain mNGβtubNeo, which expresses N-terminally tagged mNeonGreen-β-tubulin from a plasmid integrated at the β-tubulin (GL50803_101291) locus, mNeonGreen with a C18 flexible linker was amplified from pjet1.2mNG_C18 (Hardin et al., 2017) and fused to the N-terminal end of β-tubulin (GL50803_101291). Gibson assembly was used to flank the gene fusion with 200 bp sequences immediately up- and downstream of the β-tubulin gene to provide the native promoter and terminator sequences, as well as to introduce the resulting fragment into NotI- and EcoRI-digested pKS_mNeonGreen-N11_NEO (Hardin et al., 2017). The resulting plasmid, pKSmNGβtubNeo, was linearized for recombination at a unique NruI site within β-tubulin (Gourguechon and Cande, 2011) and introduced into *G. lamblia* strain WBC6 by electroporation as described above. Trophozoites containing the integrated vector with a neomycin resistance marker were selected with 150 µg/ml of the neomycin analog G418 (Sigma-Aldrich) and maintained with 600 µg/ml G418. The mNeonGreen signal in the integrated mNGβtubNeo strain is retained in the absence of G418 selection.

Stable CRISPRi-based DAP KD strains

Fourteen DAPs were selected for CRISPRi knockdown (KD) based on regional localization. To create stable KD strains, gRNAs 20 nucleotide base pairs in length targeting the non-template strand of the coding region of each gene were selected using the CRISPR Guide RNA design tool (Benchling; https://benchling.com/crispr) as previously described (McInally et al., 2019a). Selection criteria for gRNAs included the minimization of predicted off-target effects, proximity to the start codon and absence of BbsI restriction enzyme sites within the gRNA sequence. One gRNA was tested for each DAP: DAP3951 (+17R: 5′-GGCTATGTCGTACGCTAT-AA-3′), DAP4410 (+618R: 5′-ACCCAGCAACAATCGTCTCG-3′), DAP5188 (+288R: 5′-GCGGCGTCCTCCCATCTGGA-3′), DAP5489 (+23R: 5′-CATGCGGCTCACAGTGAGGG-3′), DAP5883 (+62R: 5′-

ACCGTTCTCATCGACTACAA-3′), DAP6751 (+17R: 5′-GGCTATGT-CGTACGCTATAA-3′), DAP9515 (+11R: 5′-CCAGTCTGCACTTGCC-TTAA-3′), DAP11554 (+17R: 5′-GTCACGATAGATCTGAGAGG-3′), DAP16263 (+48R: 5′-GAGACTCTAT-GAGTTTGACT-3′), DAP16342 (+44R: 5′-ACCGTTCACTTCCTCGACCA-3′), DAP17053 (+65R: 5′-C-GTGGGCAGTGCCTCCACGA-3′), DAP17551 (+11R: 5′-CCATTCCT-TAGAATCAGCTT-3′), DAP23492 (+15R: 5′-GATTTGGCGCCTCAAA-GTTG-3′), DAP40016 (+30R: 5′-CAGTGTCTCCATTAGCGTCA-3′). Annealed gRNA oligonucleotides with added four-base overhangs complementary to the ends of BbsI-digested dCas9g1pac were cloned as previously described (McInally et al., 2019a,b). The presence of the correct gRNA was confirmed using Sanger sequencing.

CRISPRi vectors (20 µg) were electroporated into *G. lamblia* strain mNGβtubNeo and selected with puromycin as described above. Two strains, DAP5188KD and DAP6751KD, with disc hyperstability defects (see Results above) were selected for further analysis after phenotypic screening; a total of three independent electroporations of each CRISPRi vector dCas5188gRNA288R, dCas6751gRNA17R and dCas9g1pac with a nonsense gRNA (nsgRNA) was performed as described previously (McInally et al., 2019a,b).

qRT-PCR of DAP gene expression in CRISPRi KD strains

Total RNA was extracted from three separate electroporations of each CRISPRi KD and nsgRNA control strain (1×10^7 trophozoites per extraction) using the Direct-Zol RNA Miniprep Kit (Zymo Research). Complementary DNA (cDNA) was generated from 1 µg of purified RNA using 5× All-In-One RT Master Mix (Applied Biological Materials). The quantitative reverse transcription (qRT)-PCR reaction was performed using *G. lamblia* cDNA from the KD or control strains (above) with the KiCqStart SYBR Green qPCR ReadyMix (Sigma) according to the manufacturer's instructions. The qRT-PCR reactions were performed with three technical replicates per condition and also included forward and reverse primers (each at a 0.3 µM final concentration) targeting the DAP5188, DAP6751 or GAPDH (positive control, GL50803_17043) genes. Primer sets were: 5188qPCR202F 5′-TACACGGCCATTATGCTTGC-3′ and 5188qPC-R373R 5′-AGATGAAGCGATTGTGGGGA-3′, 6751qPCR2442F 5′-TC-CGCAGCTATCTCAGACAG-3′ and 6751qPCR2596R 5′-CCAGGCTTA-GCGATGAAACC-3′, 17043qPCR120F 5′-CGCCATCAACAACAGGA-ACA-3′ and 17043qPCR304R 5′-ACACGGGCTTGTCATTGAAC-3′. The cDNA concentration was initially empirically determined and optimized for each primer set to minimize quantitative cycling error and variability, with 12.5 ng total used in reactions with the DAP5188 primer set, and 5 ng total used in reactions with the GAPDH and DP6751 primer sets. Quantitative RT-PCR was performed in a Roche LightCycler 480 II, with an initial melt at 95°C for 5 min, followed by 45 cycles of 95°C for 10 s, 60°C for 10 s, and 72°C for 10 s. Quantification measurements were taken during the annealing step. Following this, a melting curve was obtained by ramping from 65°C to 97°C at 0.11°C/sec. Crossing threshold (Ct) values were obtained using the Second Derivative Maximum method of calculation (Taylor et al., 2019). Quantitative data analysis was performed according to (Taylor et al., 2019). Normalized fold-expression values were averaged for three technical replicates for each of three electroporations of the same KD strain; the relative expression values (in %) for DAP5188 and DAP6751 were normalized relative to the GAPDH expression for that strain.

Immunostaining of CRISPRi KD strains

CRISPRi KD strain trophozoites (1×10^7 total cells) were immunostained as previously described (McInally et al., 2019a,b). Briefly, culture tubes were incubated on ice for 15 min and centrifuged at 900 ***g*** for 5 min. After three washes in 5 ml 1× HBS, trophozoites were resuspended in 1 ml warm 1× HBS. Aliquots (250 µl) were dispensed to warm coverslips and incubated at 37°C for 30 min in a humidified chamber to allow cells to attach. Cells were then fixed with 4% paraformaldehyde (PFA) in 1× HBS, washed three times with 2 ml PEM buffer pH 6.9 (0.1 M PIPES, 2 mM EGTA. 1 mM $MgSO_4$), quenched with 250 mM glycine and permeabilized with 0.1% Triton X-100 for 10 min. After three additional PEM washes, coverslips were blocked in 2 ml PEMBALG [100 mM PIPES pH 6.9, 1 mM EGTA, 0.1 mM $MgSO_4$, 1% BSA, 0.1% NaN_3, 100 mM lysine and 0.5% cold-water fish skin gelatin (Sigma G7765)] (Woessner and Dawson, 2012) for 30 min and incubated overnight at 4°C with anti-β-giardin (1:1000; gift from Mark Jenkins, USDA, Agricultural Research Service) and anti-CRISPRCas9 [7A9-3A3] (Abcam, ab191468, 1:1000) antibodies. Coverslips were washed three times in PEMBALG and incubated with goat anti-rabbit IgG (H+L) Cross-Adsorbed Secondary antibody Alexa Fluor 594 (A-11012, ThermoFisher/Invitrogen, 1:500) and/or goat anti-mouse IgG (H+L) Cross-Adsorbed Secondary antibody, Alexa Fluor 647 (A-11012, ThermoFisher/Invitrogen, 1:500) for 2 h at room temperature. Coverslips were then washed three times each with PEMBALG and PEM, mounted in Prolong Diamond antifade reagent (Thermo Scientific) and were allowed to cure overnight prior to imaging. Imaging was performed using differential interference contrast (DIC) and epifluorescence with a Leica DMI6000B wide-field inverted fluorescence microscope (Plan Apo 100×, NA 1.40 oil immersion objective). Optical sections were acquired at 0.2-µm intervals with a QImaging Rolera-MGi Plus EMCCD camera and MetaMorph acquisition software (MDS Analytical Technologies). Images were processed using FIJI (Schindelin et al., 2012).

Biochemical extraction and fractionation of the *G. lamblia* MT cytoskeleton

Detergent extraction of the MT cytoskeleton of *G. lamblia* was performed as previously described (Hagen et al., 2011) with several modifications (Fig. S1). Trophozoite cultures were iced and harvested as described above. Three pellets, each containing 2×10^8 cells, were washed three times with 5 ml of 1× HBS pH 7.0 (137 mM NaCl, 21 mM HEPES, 5.6 mM glucose, 5.0 mM KCl, 0.76 mM Na_2HPO_4) and centrifuged at 900 ***g*** and 4°C. To demembranate cytoskeletons, the washed pellets were resuspended in 1 ml of 0.5× HBS/1× PHEM (1× PHEM: 60 mM PIPES, 25 mM HEPES, 10 mM EGTA, 1 mM $MgCl_2$ pH 7.4) containing 1% Triton X-100, 1 M KCl and 1× HALT protease inhibitor cocktail (Roche) to prevent proteolysis. Suspensions were transferred to 1.8 ml Eppendorf tubes and vortexed continuously for 30 min (VWR Vortex-Genie2, vortex speed setting at 5) to extract the total cytoskeleton preparation 'T' (Fig. S1G). Preparation T was then centrifuged at 3000 ***g***, 25°C for 5 min. The resulting supernatant fraction was designated 'S1' and was saved for SDS-PAGE (Fig. S1G). The pellets, designated 'P1', were washed twice in 1 ml 0.5× HBS/1× PHEM lacking both 1% Triton X-100 and 1 M KCl. One P1 pellet was retained for analysis and was resuspended either in 200 µl 0.5× HBS/1× PHEM for immunostaining, negative-staining, or proteomics (Fig. S1C,D, H), or in 200 µl RIPA buffer (Sigma-Aldrich) for SDS-PAGE (Fig. S1G). The presence of intact, demembranated cytoskeletons (ventral disc with attached flagellar components) in P1 was confirmed by DIC microscopy (Fig. S1B), and immunostaining with anti-α-tubulin (anti-TAT1; Sigma-Aldrich, 0002091, 1:250) and anti-δ-giardin (gift from Mark Jenkins, USDA ARS, 1:1000) antibodies confirmed retention of the disc and flagella (Fig. S1C).

To further dissociate the cytoskeletons, the remaining two P1 pellets were resuspended in 1 ml of 10 mM Tris, 1 mM EDTA pH 7.7, incubated for 48 h at 4°C and centrifuged at 3000 ***g*** at 25°C for 5 min. The supernatant was retained for SDS-PAGE or proteomic analysis as the 'S2' fraction (Fig. S1A, G), and the 'P2' complexes were washed twice in 1 ml 10 mM Tris, 1 mM EDTA pH 7.7 and centrifuged at 3000 ***g*** as described above. One P2 pellet was resuspended in 200 µl RIPA buffer for SDS-PAGE, the second was resuspended in 1 ml of 10 mM HEPES, 5 mM EDTA pH 8.7 and incubated for an additional 48 h at 4°C. After the final incubation, the extracted complexes were centrifuged at 3000 ***g***, at 25°C for 5 min. The supernatant was retained as the 'S3' fraction, and the final 'P3' pellet was washed twice in 1 ml of 10 mM HEPES, 5 mM EDTA pH 8.7 and resuspended either in 200 µl 1× PHEM for immunostaining or proteomics or in 200 µl RIPA for SDS-PAGE. To confirm dissociation of axonemes from discs, an aliquot of the S3 fraction was immunostained using the anti-δ-giardin antibody and imaged using DIC and epifluorescence microscopy (Fig. S1E,F).

SDS-PAGE and western blotting

For SDS-PAGE of fractionated proteins (Fig. S1G), the total cytoskeletal preparation T and all supernatant fractions (S1, S2, S3) were mixed 1:1 with RIPA buffer. Aliquots (200 µl) of preparation T, supernatants S1, S2 and S3,

and of the pellets resuspended in RIPA buffer (P1, P2, P3) were then sonicated (Heat Systems W-375, duty cycle 50%, output control 2, ten pulses). Protein concentrations were determined by the Pierce BCA assay (Thermo Scientific) using a Perkin-Elmer Victor ×3 plate reader. Cell lysate samples containing 2.4 µg of total protein were run on Precise Tris·HEPES protein gels (4–20%, ThermoFisher). Protein gels were stained with Instant Blue (Expedeon) for 1 h at room temperature and were destained overnight in MilliQ water when necessary (Fig. S1G).

For western blotting of cytoskeletal preparations, cell lysate samples (20 µg total protein) were electrophoresed as described above. After separation, proteins were transferred to 0.45 µm nitrocellulose membrane (Bio-Rad) using a Bio-Rad Mini Trans-Blot cell at 100 V for 2 h on ice. Membranes were blocked for 1 h at room temperature in 5% (w/v) milk in PBS with 0.05% Tween. Antibodies were diluted in 5% (w/v) milk in PBS or TBS with 0.05% Tween as follows: mouse monoclonal antibody against hemagglutinin (HA), clone HA-7 (Sigma, H9658, 1:5000); rabbit anti-δ-giardin (gift from Mark Jenkins, USDA ARS, 1:1000); mouse monoclonal antibody against α-tubulin (TAT1; Sigma-Aldrich, 00020911, 1:2500), goat anti-mouse IgG (H+L) HRP conjugate (Bio-Rad, 170516, 1:10000); goat anti-rabbit IgG (H+L) HRP conjugate (Bio-Rad, 170515, 1:5000). Amersham ECL Prime substrate (GE Healthcare) was used for chemiluminescence detection with a ProteinSimple AlphaImager documentation system.

Mass spectrometry and proteomic analysis

Fractions P1, S2, S3 and P3 (20 µg total protein in the fractionation buffers described above) were processed at the UC Davis Genome Center Proteomics Core facility for shotgun mass spectrometry analyses. All shotgun LC-MS/MS samples were analyzed the using X! Tandem search engine [The GPM, https://www.thegpm.org; version X! Tandem Alanine (2017.2.1.4)]. X! Tandem was used to search the uniprotgiardiaintestinalis_Craprev database (14528 entries) assuming the digestion enzyme trypsin and with a fragment ion mass tolerance of 20 p.p.m. and a parent ion tolerance of 20 p.p.m. X! Tandem variable specified amino acid modifications were Glu→pyro-Glu in the N-terminus, loss of NH_3 in the N-terminus, Gln→pyro-Glu in the N-terminus, deamidation of Asp and Gln, oxidation of Met and Trp, and dioxidation of Met and Trp. Scaffold Proteome software (version 4.8.4; Proteome Software Inc., Portland, OR) was used to validate MS/M-based peptide and protein identifications. Peptide identifications were accepted if they exceeded specific thresholds of the database search engine. Protein identifications were accepted if they contained at least five identified peptides. Proteins that contained similar peptides and could not be differentiated on the basis of MS/MS analysis alone were grouped, in order to satisfy the principles of parsimony. Proteins that shared substantial peptide evidence were grouped into clusters.

Live imaging of GFP-tagged DAP strains

DAP-GFP fusion strains were thawed from frozen stocks and cultured for 24 to 48 h prior to live imaging. Cells were iced and harvested as described above, resuspended in 1 ml warm (37°C) TYI-S-33, and 300 µl aliquots were incubated in 96-well black glass-bottomed imaging plates (Cellvis, Mountain View, CA) for ≤2 h at 37°C in a nitrogen-enriched atmosphere to promote attachment. 1 ml medium was replaced with 1× HBS, and trophozoites were incubated under the same conditions for 30 min. Additional warm (37°C) 1× HBS washes were performed as needed during imaging to remove detached cells. DIC and epifluorescence imaging was performed with a Leica DMI6000B microscope as described above. Images were processed using Fiji (Schindelin et al., 2012) and 2D maximum-intensity projections were created from the 3D data sets when required.

Structured illumination microscopy

Trophozoites (1×10^7 cells) from CRISPRi strains were iced, harvested and washed twice in 5 ml 1× HBS. Live trophozoites were resuspended in 1× HBS and allowed to attach to coverslips as described above. Attached cells were fixed *in situ* with 4% PFA in 1× HBS and quenched with 250 mM glycine. Coverslips were mounted with Prolong Diamond antifade (Thermo Scientific) and allowed to cure overnight prior to imaging. 3D stacks were collected at 0.125 µm intervals on a Nikon N-SIM Structured Illumination Super-resolution Microscope with a 100×/NA 1.49 objective, 100 EX V-R diffraction grating and an Andor iXon3 DU-897E EMCCD. Raw images were acquired in the 3D-SIM format (NIS-Elements, Nikon); reconstruction used three different diffraction grating angles each with five translations. Single-channel data spanned ∼5 µm depth and required acquisition times of ∼6 min. Image reconstruction was performed in NIS-Elements.

Transmission electron microscopy

Detergent extracted cytoskeletal preparations (see above) were applied to 400 mesh formvar/carbon coated glow-discharged grids. Negative staining was performed by applying 1% PTA pH 5.4, and grids were dried by blotting without washes. For thin sections, *G. lamblia* trophozoites that had been pelleted or had attached to ACLAR discs (Electron Microscopy Sciences) were fixed for 10 min in 4% PFA and fixed again for 1 h in 1% OsO_4. Cells were washed three times with cold doubly distilled water to remove fixative, dehydrated through ascending concentrations of ethanol (30%, 50%) and incubated for 1 h in 2% uranyl acetate in 50% ethanol. Dehydration continued through 70% ethanol and three changes of 95% ethanol and was completed with three changes in 100% ethanol for a minimum of 10 min each change. Cells were embedded in 1:1 epoxy resin: acetone overnight at room temperature. The next day the resin was removed and replaced with 100% resin twice for 2 h each. The ACLAR discs were placed at the bottom of a flat bottom beam capsule with the cells facing up and the capsule was filled with fresh resin. The blocks were polymerized at 70°C overnight. The blocks were trimmed and thin sections were cut with a Leica UCT ultramicrotome (Leica Ultracut UCT, Leica, Vienna, Austria), and stained with 2% uranyl acetate in 70% ethanol plus lead citrate before viewing in the Talos L120C electron microscope (FEI Company/Thermo Scientific, Hillsboro, OR; made in Eindhoven, The Netherlands) at 100KV. Images were acquired using the fully integrated Ceta CMOS camera.

Assay of disc hyperstability in CRISPRi KD strains after detergent and high-salt extraction

To determine whether the ventral discs of KD strains retained hyperstability, trophozoites from one confluent 12 ml culture (2×10^7 cells) of each DAP KD strain were harvested, resuspended in 1 ml 0.5× HBS/1× PHEM with 1% Triton X-100 and 2 M KCl and extracted with vortex mixing as described previously for fractionation of the cytoskeleton. P1 was resuspended in 200 µl 0.5× HBS/1× PHEM. For imaging, ∼100 µl of each detergent extracted cytoskeletal preparation was added to poly-L-lysine treated coverslips and allowed to settle for 15 min. The adhered cytoskeletons were fixed with 4% PFA in 1× HBS for 2 min and quenched with 250 mM glycine for 5 min. Coverslips were mounted on slides using Prolong Diamond antifade mounting medium and cured overnight. Cytoskeletons were examined with a Leica DMI 6000B fluorescence microscope and *z*-stacks of random fields were acquired. For scoring and presentation, 2D projections were created from acquired *z*-stacks. Twelve CRISPRi-mediated DAP KD strains that lacked aberrant disc phenotypes with this assay were excluded from further analysis. For DAP5188KD, DAP6751KD and the nsgRNA control strains, an average of 120 cytoskeletons were counted and evaluated for each independent electroporation (biological replicate).

For quantification of aberrant ventral discs, cytoskeletons were scored and assigned to six categories based on phenotype. Discs with a wild-type appearance had an intact overlap zone and an encircled bare area. 'Unhinged' discs lacked an intact overlap zone. Discs in the 'point' category were flattened and lacked an overlap zone, yet two tips of the disc spiral still touched at a single point. 'Horseshoe' discs lacked an overlap zone and had an opened bare area region no longer surrounded by disc MTs. The 'fragmented' category includes discs that were largely intact but had gaps or portions missing from the disc spiral. 'Small' describes discs with an enclosed, small bare area, lacking MTs on the outer half perimeter of the disc. Discs that did not clearly fall into one of the categories or were unscoreable (e.g. discs stacked upon each other, discs at an angle, or discs obscured by inorganic matter) were excluded from the count.

Assay of disc MT dynamics in CRISPRi KD strains using nocodazole or Taxol

For analyses of MT dynamics, the stable CRISPRi KD strain DAP5188KD and the control strain carrying a non-specific gRNA (nsgRNA) were thawed

and grown for 24 h at 37°C in TYI-S-33 medium. Cultures (12 ml) were then incubated on ice for 15 min, divided equally into two 8 ml screw-cap tubes (Fisher Scientific) and grown for an additional 16 h at 37°C. Following this incubation, one tube was incubated with a final concentration of 10 µM nocodazole in DMSO for 5 h, while the remaining tube was incubated with DMSO alone. Alternatively, one tube was incubated with 20 µM Taxol in DMSO for 1 h and the remaining tube was incubated with DMSO alone. Cells were then chilled for 15 min at 4°C and harvested by centrifugation (900 ***g***). The medium was decanted and pellets were washed three times with 1× HBS (4°C). After the final centrifugation step, the cell pellet was resuspended in 0.5 ml 1× HBS. Prior to imaging, trophozoites were allowed to attach to coverslips for 15 min at 37°C, then fixed in a final concentration of 4% PFA in 1× HBS for 2 min. Fixation was quenched by incubating coverslips in 250 mM glycine for 5 min. Coverslips were mounted on slides using Prolong Diamond antifade mountant and slides were cured overnight prior to imaging with a Leica DMI 6000B wide-field microscope as described above. For both the DAP5188KD and the nsgRNA control strain, three independent electroporations were imaged and scored. Images were captured of random fields and blind slide reading was performed to minimize investigator bias. Disc phenotypes were then scored for every trophozoite in a given frame. An average of 165 cells per electroporation were imaged.

Disc phenotypes following nocodazole treatment were assigned to six categories that described the range of variation of visually observable aberrant ventral disc MT architecture. As 'wild-type' discs are insensitive to nocodazole, they retained an intact 3D architecture with an overlap zone and a completely encircled bare area. 'Dissociated' discs were completely disrupted; cells in this category retained tubulin fluorescence in the anterior of the cell but lacked any disc structure whatsoever. 'Half discs' were those that had close to one half of the disc missing on the anterior-posterior axis. The 'partial' disc category included discs in which portions of the spiral were dissociated or fragmented. 'Horseshoe' category discs had an open and flattened U-shaped conformation with the bare area no longer enclosed. Lastly, 'unhinged' discs were flattened and lacked an intact overlap zone, which allowed the upper and sides of the disc to twist or rotate freely.

Acknowledgements
We thank Dr Alex Paredez (University of Washington, Seattle, WA) for plasmids pjet1.2-mNeonGreen_C18 and pKS_mNeonGreen-N11_NEO, and Dr Mark Jenkins (U.S. Department of Agriculture, Agricultural Research Service, Parasitic Diseases Laboratory) for *G. lamblia* anti-β-giardin and anti-δ-giardin antibodies. We thank Dr Michael Paddy (UC Davis MCB Microscopy Imaging Facility, UC Davis Campus Core Research Facility) for helpful advice and use of the 3i SDC and Nikon N-SIM microscopes. We also thank Patricia Kysar (UC Davis MCB Electron Microscopy Lab) for advice and TEM training and Michelle Salemi and Dr Brett Phinney (UCD Proteomics Core) for assistance with mass spectroscopy.

Competing interests
The authors declare no competing or financial interests.

Author contributions
Conceptualization: C.N., K.D.H., N.H., S.C.D.; Methodology: C.N., K.D.H., N.H., T.M.C., K.J., R.L., K.N.; Validation: C.N., K.D.H., N.H., T.M.C., R.L., K.N.; Formal analysis: C.N., K.D.H., N.H., S.C.D.; Investigation: C.N., K.D.H., N.H., T.M.C., S.C.D.; Resources: C.N., K.D.H., N.H., T.M.C.; Data curation: C.N., K.D.H., N.H., S.C.D.; Writing - original draft: C.N., K.D.H., N.H., S.C.D.; Writing - review & editing: C.N., K.D.H., N.H., S.C.D.; Visualization: C.N., K.D.H., N.H., K.N., S.C.D.; Supervision: S.C.D.; Project administration: S.C.D.; Funding acquisition: S.C.D.

Funding
This work was supported by the National Institutes of Health (grant number: NIH 5R01AI077571-11 to S.C.D.) and the Center for Comparative Medicine at University of California Davis School of Medicine (grant number: T32 AI060555 Animal Models of Infectious Diseases Training Program to C.N). Deposited in PMC for release after 12 months.

Data availability
Mass spectrometry data from each of the disc fractionations are deposited in the MassIVE database, with accession number MSV000085943.

Supplementary information
Supplementary information available online at
https://jcs.biologists.org/lookup/doi/10.1242/jcs.227355.supplemental

References
Akhmanova, A. and Hoogenraad, C. C. (2005). Microtubule plus-end-tracking proteins: mechanisms and functions. *Curr. Opin. Cell Biol.* **17**, 47-54. doi:10.1016/j.ceb.2004.11.001

Akhmanova, A. and Steinmetz, M. O. (2015). Control of microtubule organization and dynamics: two ends in the limelight. *Nat. Rev. Mol. Cell Biol.* **16**, 711-726. doi:10.1038/nrm4084

Amos, L. A. (2004). Microtubule structure and its stabilisation. *Org. Biomol. Chem.* **2**, 2153-2160. doi:10.1039/b403634d

Amos, L. A. (2008). The tektin family of microtubule-stabilizing proteins. *Genome Biol.* **9**, 229. doi:10.1186/gb-2008-9-7-229

Andersson, J. O., Sjögren, A. M., Horner, D. S., Murphy, C. A., Dyal, P. L., Svärd, S. G., Logsdon, J. M., Jr, Ragan, M. A., Hirt, R. P. and Roger, A. J. (2007). A genomic survey of the fish parasite Spironucleus salmonicida indicates genomic plasticity among diplomonads and significant lateral gene transfer in eukaryote genome evolution. *BMC Genomics* **8**, 51. doi:10.1186/1471-2164-8-51

Baker, D. A., Holberton, D. V. and Marshall, J. (1988). Sequence of a giardin subunit cDNA from *Giardia lamblia*. *Nucleic Acids Res.* **16**, 7177. doi:10.1093/nar/16.14.7177

Bauer, B., Engelbrecht, S., Bakker-Grunwald, T. and Scholze, H. (1999). Functional identification of alpha 1-giardin as an annexin of *Giardia lamblia*. *FEMS Microbiol. Lett.* **173**, 147-153. doi:10.1111/j.1574-6968.1999.tb13496.x

Bennett, V. and Davis, J. (1981). Erythrocyte ankyrin: immunoreactive analogues are associated with mitotic structures in cultured cells and with microtubules in brain. *Proc. Natl. Acad. Sci. USA* **78**, 7550-7554. doi:10.1073/pnas.78.12.7550

Bowne-Anderson, H., Hibbel, A. and Howard, J. (2015). Regulation of microtubule growth and catastrophe: unifying theory and experiment. *Trends Cell Biol.* **25**, 769-779. doi:10.1016/j.tcb.2015.08.009

Brown, J. R., Schwartz, C. L., Heumann, J. M., Dawson, S. C. and Hoenger, A. (2016). A detailed look at the cytoskeletal architecture of the *Giardia lamblia* ventral disc. *J. Struct. Biol.* **194**, 38-48. doi:10.1016/j.jsb.2016.01.011

Cheissin, E. M. (1964). Ultrastructure of lamblia duodenalis. I. Body surface, sucking disc and median bodies. *J. Protozool.* **11**, 91-98. doi:10.1111/j.1550-7408.1964.tb01725.x

Crossley, R. and Holberton, D. V. (1983a). Characterization of proteins from the cytoskeleton of *Giardia lamblia*. *J. Cell Sci.* **59**, 81-103.

Crossley, R. and Holberton, D. V. (1983b). Selective extraction with Sarkosyl and repolymerization in vitro of cytoskeleton proteins from *Giardia*. *J. Cell Sci.* **62**, 419-438.

Crossley, R. and Holberton, D. V. (1985). Assembly of 2.5 nm filaments from giardin, a protein associated with cytoskeletal microtubules in *Giardia*. *J. Cell Sci.* **78**, 205-231.

Cyrklaff, M., Kudryashev, M., Leis, A., Leonard, K., Baumeister, W., Menard, R., Meissner, M. and Frischknecht, F. (2007). Cryoelectron tomography reveals periodic material at the inner side of subpellicular microtubules in apicomplexan parasites. *J. Exp. Med.* **204**, 1281-1287. doi:10.1084/jem.20062405

Davids, B. J., Gilbert, M. A., Liu, Q., Reiner, D. S., Smith, A. J., Lauwaet, T., Lee, C., McArthur, A. G. and Gillin, F. D. (2011). An atypical proprotein convertase in *Giardia lamblia* differentiation. *Mol. Biochem. Parasitol.* **175**, 169-180. doi:10.1016/j.molbiopara.2010.11.008

Davids, B. J., Williams, S., Lauwaet, T., Palanca, T. and Gillin, F. D. (2008). *Giardia lamblia* aurora kinase: a regulator of mitosis in a binucleate parasite. *Int. J. Parasitol.* **38**, 353-369. doi:10.1016/j.ijpara.2007.08.012

Davis, J. Q. and Bennett, V. (1984). Brain ankyrin. A membrane-associated protein with binding sites for spectrin, tubulin, and the cytoplasmic domain of the erythrocyte anion channel. *J. Biol. Chem.* **259**, 13550-13559.

Dawson, S. C. and House, S. A. (2010). Imaging and analysis of the microtubule cytoskeleton in giardia. *Methods Cell Biol.* **97**, 307-339. doi:10.1016/S0091-679X(10)97017-9

Dawson, S. C. and Paredez, A. R. (2013). Alternative cytoskeletal landscapes: cytoskeletal novelty and evolution in basal excavate protists. *Curr. Opin. Cell Biol.* **25**, 134-141. doi:10.1016/j.ceb.2012.11.005

Dawson, S. C., Sagolla, M. S., Mancuso, J. J., Woessner, D. J., House, S. A., Fritz-Laylin, L. and Cande, W. Z. (2007). Kinesin-13 regulates flagellar, interphase, and mitotic microtubule dynamics in Giardia intestinalis. *Eukaryot. Cell* **6**, 2354-2364. doi:10.1128/EC.00128-07

Ebneter, J. A. and Hehl, A. B. (2014). The single epsin homolog in *Giardia lamblia* localizes to the ventral disk of trophozoites and is not associated with clathrin membrane coats. *Mol. Biochem. Parasitol.* **197**, 24-27. doi:10.1016/j.molbiopara.2014.09.008

Egydio de Carvalho, C., Tanaka, H., Iguchi, N., Ventela, S., Nojima, H. and Nishimune, Y. (2002). Molecular cloning and characterization of a complementary DNA encoding sperm tail protein SHIPPO 1. *Biol. Reprod.* **66**, 785-795. doi:10.1095/biolreprod66.3.785

Einarsson, E., Ma'ayeh, S. and Svard, S. G. (2016). An up-date on Giardia and giardiasis. *Curr. Opin. Microbiol.* **34**, 47-52. doi:10.1016/j.mib.2016.07.019
Ellis, J. G., Davila, M. and Chakrabarti, R. (2003). Potential involvement of extracellular signal-regulated kinase 1 and 2 in encystation of a primitive eukaryote, *Giardia lamblia*. Stage-specific activation and intracellular localization. *J. Biol. Chem.* **278**, 1936-1945. doi:10.1074/jbc.M209274200
Elmendorf, H. G., Dawson, S. C. and McCaffery, J. M. (2003). The cytoskeleton of *Giardia lamblia*. *Int. J. Parasitol.* **33**, 3-28. doi:10.1016/S0020-7519(02)00228-X
Feely, D. E., Schollmeyer, J. V. and Erlandsen, S. L. (1982). *Giardia* spp.: distribution of contractile proteins in the attachment organelle. *Exp. Parasitol.* **53**, 145-154. doi:10.1016/0014-4894(82)90100-X
Feely, D. E., Hoberton, D. V. and Erlandsen, S. L. (1990). The biology of *Giardia*. In *Giardiasis*, Vol. 3 (ed. E. A. Meyer), pp. 11-50. Amsterdam: Elsevier.
Francia, M. E., Jordan, C. N., Patel, J. D., Sheiner, L., Demerly, J. L., Fellows, J. D., de Leon, J. C., Morrissette, N. S., Dubremetz, J.-F. and Striepen, B. (2012). Cell division in Apicomplexan parasites is organized by a homolog of the striated rootlet fiber of algal flagella. *PLoS Biol.* **10**, e1001444. doi:10.1371/journal.pbio.1001444
Friend, D. S. (1966). The fine structure of *Giardia muris*. *J. Cell Biol.* **29**, 317-332. doi:10.1083/jcb.29.2.317
Fry, A. M., Bayliss, R. and Roig, J. (2017). Mitotic regulation by NEK KINASE NETWorks. *Front. Cell Dev. Biol.* **5**, 102. doi:10.3389/fcell.2017.00102
Garnham, C. P. and Roll-Mecak, A. (2012). The chemical complexity of cellular microtubules: tubulin post-translational modification enzymes and their roles in tuning microtubule functions. *Cytoskeleton (Hoboken)* **69**, 442-463. doi:10.1002/cm.21027
Gourguechon, S. and Cande, W. Z. (2011). Rapid tagging and integration of genes in Giardia intestinalis. *Eukaryot. Cell* **10**, 142-145. doi:10.1128/EC.00190-10
Hagen, K. D., Hirakawa, M. P., House, S. A., Schwartz, C. L., Pham, J. K., Cipriano, M. J., De La Torre, M. J., Sek, A. C., Du, G., Forsythe, B. M. et al. (2011). Novel structural components of the ventral disc and lateral crest in Giardia intestinalis. *PLoS Negl. Trop. Dis.* **5**, e1442. doi:10.1371/journal.pntd.0001442
Hansen, W. R., Tulyathan, O., Dawson, S. C., Cande, W. Z. and Fletcher, D. A. (2006). Giardia lamblia attachment force is insensitive to surface treatments. *Eukaryot. Cell* **5**, 781-783. doi:10.1128/EC.5.4.781-783.2006
Hardin, W. R., Li, R., Xu, J., Shelton, A. M., Alas, G. C. M., Minin, V. N. and Paredez, A. R. (2017). Myosin-independent cytokinesis in Giardia utilizes flagella to coordinate force generation and direct membrane trafficking. *Proc. Natl. Acad. Sci. USA* **114**, E5854-E5863. doi:10.1073/pnas.1705096114
Hoebeke, J., Van Nijen, G. and De Brabander, M. (1976). Interaction of oncodazole (R 17934), a new antitumoral drug, with rat brain tubulin. *Biochem. Biophys. Res. Commun.* **69**, 319-324. doi:10.1016/0006-291X(76)90524-6
Holberton, D. V. (1973). Fine structure of the ventral disk apparatus and the mechanism of attachment in the flagellate *Giardia muris*. *J. Cell Sci.* **13**, 11-41.
Holberton, D. V. (1974). Attachment of *Giardia*-a hydrodynamic model based on flagellar activity. *J. Exp. Biol.* **60**, 207-221.
Holberton, D. V. (1981). Arrangement of subunits in microribbons from *Giardia*. *J. Cell Sci.* **47**, 167-185.
Holberton, D. V. and Ward, A. P. (1981). Isolation of the cytoskeleton from *Giardia*. Tubulin and a low-molecular-weight protein associated with microribbon structures. *J. Cell Sci.* **47**, 139-166.
House, S. A., Richter, D. J., Pham, J. K. and Dawson, S. C. (2011). Giardia flagellar motility is not directly required to maintain attachment to surfaces. *PLoS Pathog.* **7**, e1002167. doi:10.1371/journal.ppat.1002167
Hu, K., Johnson, J., Florens, L., Fraunholz, M., Suravajjala, S., DiLullo, C., Yates, J., Roos, D. S. and Murray, J. M. (2006). Cytoskeletal components of an invasion machine–the apical complex of Toxoplasma gondii. *PLoS Pathog.* **2**, e13. doi:10.1371/journal.ppat.0020013
Ichikawa, M. and Bui, K. H. (2018). Microtubule inner proteins: a meshwork of luminal proteins stabilizing the doublet microtubule. *BioEssays* **40**, 1700209. doi:10.1002/bies.201700209
Jenkins, M. C., O'Brien, C. N., Murphy, C., Schwarz, R., Miska, K., Rosenthal, B. and Trout, J. M. (2009). Antibodies to the ventral disc protein δ-giardin prevent in vitro binding of *Giardia lamblia* trophozoites. *J. Parasitol.* **95**, 895-899. doi:10.1645/GE-1851R.1
Kaczmarzyk, D., Cengic, I., Yao, L. and Hudson, E. P. (2018). Diversion of the long-chain acyl-ACP pool in Synechocystis to fatty alcohols through CRISPRi repression of the essential phosphate acyltransferase PlsX. *Metab. Eng.* **45**, 59-66. doi:10.1016/j.ymben.2017.11.014
Kim, J. and Park, S.-J. (2019). Role of gamma-giardin in ventral disc formation of *Giardia lamblia*. *Parasit. Vectors* **12**, 227. doi:10.1186/s13071-019-3478-8
Larson, M. H., Gilbert, L. A., Wang, X., Lim, W. A., Weissman, J. S. and Qi, L. S. (2013). CRISPR interference (CRISPRi) for sequence-specific control of gene expression. *Nat. Protoc.* **8**, 2180-2196. doi:10.1038/nprot.2013.132
Lauwaet, T., Davids, B. J., Torres-Escobar, A., Birkeland, S. R., Cipriano, M. J., Preheim, S. P., Palm, D., Svärd, S. G., McArthur, A. G. and Gillin, F. D. (2007). Protein phosphatase 2A plays a crucial role in *Giardia lamblia* differentiation. *Mol. Biochem. Parasitol.* **152**, 80-89. doi:10.1016/j.molbiopara.2006.12.001
Lauwaet, T., Smith, A. J., Reiner, D. S., Romijn, E. P., Wong, C. C. L., Davids, B. J., Shah, S. A., Yates, J. R., III and Gillin, F. D. (2011). Mining the *Giardia* genome and proteome for conserved and unique basal body proteins. *Int. J. Parasitol.* **41**, 1079-1092. doi:10.1016/j.ijpara.2011.06.001
Li, J., Mahajan, A. and Tsai, M.-D. (2006). Ankyrin repeat: a unique motif mediating protein-protein interactions. *Biochemistry* **45**, 15168-15178. doi:10.1021/bi062188q
Linck, R., Fu, X., Lin, J., Ouch, C., Schefter, A., Steffen, W., Warren, P. and Nicastro, D. (2014). Insights into the structure and function of ciliary and flagellar doublet microtubules: tektins, Ca2+-binding proteins, and stable protofilaments. *J. Biol. Chem.* **289**, 17427-17444. doi:10.1074/jbc.M114.568949
Lindquist, H. D. (1996). Induction of albendazole resistance in *Giardia lamblia*. *Microb. Drug Resist.* **2**, 433-434. doi:10.1089/mdr.1996.2.433
Liu, X., Gallay, C., Kjos, M., Domenech, A., Slager, J., van Kessel, S. P., Knoops, K., Sorg, R. A., Zhang, J. R. and Veening, J. W. (2017). High-throughput CRISPRi phenotyping identifies new essential genes in Streptococcus pneumoniae. *Mol. Syst. Biol.* **13**, 931. doi:10.15252/msb.20167449
Long, S., Anthony, B., Drewry, L. L. and Sibley, L. D. (2017). A conserved ankyrin repeat-containing protein regulates conoid stability, motility and cell invasion in Toxoplasma gondii. *Nat. Commun.* **8**, 2236. doi:10.1038/s41467-017-02341-2
Lourenço, D., Andrade Ida, S., Terra, L. L., Guimarães, P. R., Zingali, R. B. and de Souza, W. (2012). Proteomic analysis of the ventral disc of *Giardia lamblia*. *BMC Res. Notes* **5**, 41. doi:10.1186/1756-0500-5-41
Manning, G., Reiner, D. S., Lauwaet, T., Dacre, M., Smith, A., Zhai, Y., Svard, S. and Gillin, F. D. (2011). The minimal kinome of Giardia lamblia illuminates early kinase evolution and unique parasite biology. *Genome Biol.* **12**, R66. doi:10.1186/gb-2011-12-7-r66
McInally, S. G., Hagen, K. D., Nosala, C., Williams, J., Nguyen, K., Booker, J., Jones, K. and Dawson, S. (2019a). Robust and stable transcriptional repression in *Giardia* using CRISPRi. *Mol. Biol. Cell* **30**, 119-130. doi:10.1091/mbc.E18-09-0605
McInally, S. G., Kondev, J. and Dawson, S. C. (2019b). Length-dependent disassembly maintains four different flagellar lengths in Giardia. *Elife* **8**, e48694. doi:10.7554/eLife.48694
Mitchison, T. and Kirschner, M. (1984). Dynamic instability of microtubule growth. *Nature* **312**, 237-242. doi:10.1038/312237a0
Morgan, U. M., Reynoldson, J. A. and Thompson, R. C. (1993). Activities of several benzimidazoles and tubulin inhibitors against Giardia spp. in vitro. *Antimicrob. Agents Chemother.* **37**, 328-331. doi:10.1128/AAC.37.2.328
Morrison, H. G., McArthur, A. G., Gillin, F. D., Aley, S. B., Adam, R. D., Olsen, G. J., Best, A. A., Cande, W. Z., Chen, F., Cipriano, M. J. et al. (2007). Genomic minimalism in the early diverging intestinal parasite *Giardia lamblia*. *Science* **317**, 1921-1926. doi:10.1126/science.1143837
Nabi, A., Yano, J., Valentine, M. S., Picariello, T. and Van Houten, J. L. (2019). SF-Assemblin genes in Paramecium: phylogeny and phenotypes of RNAi silencing on the ciliary-striated rootlets and surface organization. *Cilia* **8**, 2. doi:10.1186/s13630-019-0062-y
Nohria, A., Alonso, R. A. and Peattie, D. A. (1992). Identification and characterization of gamma giardin and the gamma giardin gene from *Giardia lamblia*. *Mol. Biochem. Parasitol.* **56**, 27-37. doi:10.1016/0166-6851(92)90151-9
Nosala, C. and Dawson, S. C. (2015). The critical role of the Cytoskeleton in the pathogenesis of giardia. *Curr. Clin. Microbiol. Rep.* **2**, 155-162. doi:10.1007/s40588-015-0026-y
Nosala, C., Hagen, K. D. and Dawson, S. C. (2018). 'Disc-o-Fever': getting down with giardia's groovy microtubule organelle. *Trends Cell Biol.* **28**, 99-112. doi:10.1016/j.tcb.2017.10.007
Owa, M., Uchihashi, T., Haruaki, H., Yamano, T., Iguchi, H., Fukuzawa, H., Wakabayashi, K., Ando, T. and Kikkawa, M. (2018). Inner lumen proteins stabilize doublet microtubules in cilia/flagella. *Nat. Commun.* **10**, 1143. doi:10.1038/s41467-019-09051-x
Palm, J. E. D., Weiland, M. E. L., Griffiths, W. J., Ljungstrom, I. and Svard, S. G. (2003). Identification of immunoreactive proteins during acute human giardiasis. *J. Infect. Dis.* **187**, 1849-1859. doi:10.1086/375356
Palm, D., Weiland, M., McArthur, A. G., Winiecka-Krusnell, J., Cipriano, M. J., Birkeland, S. R., Pacocha, S. E., Davids, B., Gillin, F., Linder, E. et al. (2005). Developmental changes in the adhesive disk during *Giardia* differentiation. *Mol. Biochem. Parasitol.* **141**, 199-207. doi:10.1016/j.molbiopara.2005.03.005
Peattie, D. A. (1990). The giardins of *Giardia lamblia*: genes and proteins with promise. *Parasitol. Today* **6**, 52-56. doi:10.1016/0169-4758(90)90070-K
Pecqueur, L., Duellberg, C., Dreier, B., Jiang, Q., Wang, C., Plückthun, A., Surrey, T., Gigant, B. and Knossow, M. (2012). A designed ankyrin repeat protein selected to bind to tubulin caps the microtubule plus end. *Proc. Natl. Acad. Sci. USA* **109**, 12011-12016. doi:10.1073/pnas.1204129109
Piatek, A., Ali, Z., Baazim, H., Li, L., Abulfaraj, A., Al-Shareef, S., Aouida, M. and Mahfouz, M. M. (2015). RNA-guided transcriptional regulation in planta via synthetic dCas9-based transcription factors. *Plant Biotechnol. J.* **13**, 578-589. doi:10.1111/pbi.12284
Preisner, H., Karin, E. L., Poschmann, G., Stuhler, K., Pupko, T. and Gould, S. B. (2016). The cytoskeleton of parabasalian parasites comprises proteins that share properties common to intermediate filament proteins. *Protist* **167**, 526-543. doi:10.1016/j.protis.2016.09.001

Russell, J. J., Theriot, J. A., Sood, P., Marshall, W. F., Landweber, L. F., Fritz-Laylin, L., Polka, J. K., Oliferenko, S., Gerbich, T., Gladfelter, A. et al. (2017). Non-model model organisms. *BMC Biol.* **15**, 55. doi:10.1186/s12915-017-0391-5

Schindelin, J., Arganda-Carreras, I., Frise, E., Kaynig, V., Longair, M., Pietzsch, T., Preibisch, S., Rueden, C., Saalfeld, S., Schmid, B. et al. (2012). Fiji: an open-source platform for biological-image analysis. *Nat. Methods* **9**, 676-682. doi:10.1038/nmeth.2019

Schwartz, C. L., Heumann, J. M., Dawson, S. C. and Hoenger, A. (2012). A detailed, hierarchical study of *Giardia lamblia's* ventral disc reveals novel microtubule-associated protein complexes. *PLoS ONE* **7**, e43783. doi:10.1371/journal.pone.0043783

Smith, I., Greenside, P. G., Natoli, T., Lahr, D. L., Wadden, D., Tirosh, I., Narayan, R., Root, D. E., Golub, T. R., Subramanian, A. et al. (2017). Evaluation of RNAi and CRISPR technologies by large-scale gene expression profiling in the Connectivity Map. *PLoS Biol.* **15**, e2003213. doi:10.1371/journal.pbio.2003213

Stoddard, D., Zhao, Y., Bayless, B. A., Gui, L., Louka, P., Dave, D., Suryawanshi, S., Tomasi, R. F.-X., Dupuis-Williams, P., Baroud, C. N. et al. (2018). Tetrahymena RIB72A and RIB72B are microtubule inner proteins in the ciliary doublet microtubules. *Mol. Biol. Cell* **29**, 2566-2577. doi:10.1091/mbc.E18-06-0405

Stojic, L., Lun, A. T. L., Mangei, J., Mascalchi, P., Quarantotti, V., Barr, A. R., Bakal, C., Marioni, J. C., Gergely, F. and Odom, D. T. (2018). Specificity of RNAi, LNA and CRISPRi as loss-of-function methods in transcriptional analysis. *Nucleic Acids Res.* **46**, 5950-5966. doi:10.1093/nar/gky437

Tao, W., Lv, L. and Chen, G.-Q. (2017). Engineering Halomonas species TD01 for enhanced polyhydroxyalkanoates synthesis via CRISPRi. *Microb Cell Fact* **16**, 48. doi:10.1186/s12934-017-0655-3

Taylor, S. C., Nadeau, K., Abbasi, M., Lachance, C., Nguyen, M. and Fenrich, J. (2019). The ultimate qPCR experiment: producing publication quality, reproducible data the first time. *Trends Biotechnol.* **37**, 761-774. doi:10.1016/j.tibtech.2018.12.002

Tůmová, P., Kulda, J. and Nohýnková, E. (2007). Cell division of *Giardia intestinalis*: assembly and disassembly of the adhesive disc, and the cytokinesis. *Cell Motil. Cytoskeleton* **64**, 288-298. doi:10.1002/cm.20183

Upcroft, J., Mitchell, R., Chen, N. and Upcroft, P. (1996). Albendazole resistance in Giardia is correlated with cytoskeletal changes but not with a mutation at amino acid 200 in beta-tubulin. *Microb. Drug Resist.* **2**, 303-308. doi:10.1089/mdr.1996.2.303

Weber, K., Geisler, N., Plessmann, U., Bremerich, A., Lechtreck, K. F. and Melkonian, M. (1993). SF-assemblin, the structural protein of the 2-nm filaments from striated microtubule associated fibers of algal flagellar roots, forms a segmented coiled coil. *J. Cell Biol.* **121**, 837-845. doi:10.1083/jcb.121.4.837

Weiland, M. E.-L., Palm, J. E., Griffiths, W. J., McCaffery, J. M. and Svärd, S. G. (2003). Characterisation of alpha-1 giardin: an immunodominant *Giardia lamblia* annexin with glycosaminoglycan-binding activity. *Int. J. Parasitol.* **33**, 1341-1351. doi:10.1016/S0020-7519(03)00201-7

Weiland, M. E.-L., McArthur, A. G., Morrison, H. G., Sogin, M. L. and Svärd, S. G. (2005). Annexin-like alpha giardins: a new cytoskeletal gene family in *Giardia lamblia*. *Int. J. Parasitol.* **35**, 617-626. doi:10.1016/j.ijpara.2004.12.009

Weisbrich, A., Honnappa, S., Jaussi, R., Okhrimenko, O., Frey, D., Jelesarov, I., Akhmanova, A. and Steinmetz, M. O. (2007). Structure-function relationship of CAP-Gly domains. *Nat. Struct. Mol. Biol.* **14**, 959-967. doi:10.1038/nsmb1291

Woessner, D. J. and Dawson, S. C. (2012). The Giardia median body protein is a ventral disc protein that is critical for maintaining a domed disc conformation during attachment. *Eukaryot. Cell* **11**, 292-301. doi:10.1128/EC.05262-11

Zhang, B., Liu, Z.-Q., Liu, C. and Zheng, Y.-G. (2016). Application of CRISPRi in Corynebacterium glutamicum for shikimic acid production. *Biotechnol. Lett.* **38**, 2153-2161. doi:10.1007/s10529-016-2207-z

Zuberi, A., Misba, L. and Khan, A. U. (2017). CRISPR Interference (CRISPRi) Inhibition of luxS Gene Expression in E. coli: An Approach to Inhibit Biofilm. *Front. Cell Infect. Microbiol.* **7**, 214. doi:10.3389/fcimb.2017.00214